AIAA Guidance, Navigation, and Control Conference and Exhibit
21 - 24 August 2006, Keystone, Colorado

AIAA 2006-6316

Trajectory Control for Very Flexible Aircraft

Christopher M. Shearer * and Carlos E. S. Cesnik †
The University of Michigan, Ann Arbor, Michigan, 48109, USA

This paper focuses on trajectory control of the 6-DOF body fixed reference frame located on a very flexible aircraft. The 6-DOF equations of motion of a reference point on the aircraft are coupled with the aeroelastic equations that govern the geometrically nonlinear structural response of the vehicle. A low-order strain-based nonlinear structural analysis coupled with unsteady finite-state potential flow aerodynamics form the basis for the aeroelastic model. The nonlinear beam finite element structural model assumes constant strain over an element in extension, twist, and in/out of plane bending. The geometrically nonlinear structural formulation, the finite state aerodynamic model, and the nonlinear rigid body equations together provide a low-order complete nonlinear aircraft analysis tool. Due to the inherent flexibility of the aircraft modeling, the low order structural frequencies are of the same order as the rigid body modes. This creates a coupling which cannot be separated by previous control schemes. The flexibility must be accounted for directly in the controller development. To accomplish this a heuristic approach based upon pilot behavior is developed. This approach separates the problem into two parts: a fast inner-loop and a slower outer-loop. Dominant kinematic nonlinearities are handled in the outer-loop while the inner loop is further separated into a lateral and longitudinal motion. Control of the inner-loop lateral motion is accomplished using a standard Linear Quadratic Regulator. For the longitudinal motion Dynamic Inversion is utilized. Differences between the desired and actual trajectories are handled in the nonlinear outer-loop using traditional proportional-integral-derivative design guidelines. The closed loop time integration is accomplished using an implicit modified Newmark method. Numerical simulations are presented highlighting the strengths and weaknesses of the method.

I. Introduction

On 17 December 1903, the Wright brothers set about the task of launching an airplane into the sky. Their multiple successes that day have been hailed as the start of heavier than air powered flight. One of the key features of their aircraft was the use of wing flexibility for roll control. Due to the low dynamic pressure seen on that flight and the relatively high stiffness to mass ratio of the aircraft, the Wright's were able to develop the required control power without any detrimental aeroelastic effects. However almost a 100 years later on 26 June 2003, NASA's Helios aircraft,[1]

> HP03-2 took off at 10:06am local time from the Navys Pacific Missile Range Facility (PMRF) located on the island of Kauai, Hawaii. ... At 10:22am and 10:24am, the aircraft encountered turbulence and the wing dihedral became much larger than normal and mild pitch oscillations began, but quickly damped out. At about 30 minutes into the flight, the aircraft encountered turbulence and morphed into an unexpected, persistent, high dihedral configuration. As a result of the persistent high dihedral, the aircraft became unstable in a very divergent pitch mode in which the airspeed excursions from the nominal flight speed about doubled every cycle of the oscillation. The aircrafts design airspeed was subsequently exceeded and the resulting high dynamic pressures caused the wing leading edge secondary structure on the outer wing panels to fail and the solar cells and skin on the upper surface of the wing to rip off. The aircraft impacted the ocean within the confines of the PMRF test range and was destroyed. ... The root causes of the mishap include: [a] Lack of adequate analysis methods led to an inaccurate risk assessment

*Major, USAF, PhD Candidate, Student Member, shearerc@umich.edu.
†Associate Professor of Aerospace Engineering, AIAA Associate Fellow, cesnik@umich.edu.

> of the effects of configuration changes leading to an inappropriate decision to fly an aircraft configuration highly sensitive to disturbances [, and] configuration changes to the aircraft, driven by programmatic and technological constraints, altered the aircraft from a spanloader to a highly point-loaded mass distribution on the same structure significantly reducing design robustness and margins of safety.

The Helios accident highlighted our limited understanding and limited analytical tools necessary for designing very flexible aircraft which have and potentially exploit aircraft flexibility. The number one root cause/recomendation from NASA[1] was a

> [That] more advanced, multidisciplinary (structures, aeroelastic, aerodynamics, atmospheric, materials, propulsion, controls, etc) time-domain analysis methods appropriate to highly flexible, morphing vehicles [be developed].

Despite the lack of fundamental understanding on the behavior of these vehicles, recent advances in airborne sensors and communication packages have brought the need for high-altitude long-endurance (HALE) aircraft. These platforms can be categorized under three broad missions, supporting either the military or civilian communities. The missions include airborne Intelligence, Surveillance, and Reconnaissance (ISR), for the military,[2] network communication nodes for the military and civilian usage,[3] and general atmospheric research.[3] Due to the mission requirements, the desired vehicles are characterized by high-aspect-ratio wings and slender fuselages, resulting in very flexible vehicles. Examples of mission optimization studies for this class of vehicle can be found in Ref. 2, where it is shown the aircraft are required to have a fuel fraction greater than 66%. This results in a very small structural weight fraction. The combination of high aerodynamic efficiency and low structural weight fraction yields inherently flexible wings and nonlinear structural and flight dynamics. The HALE vehicle will then be susceptible to large dynamic wing deformations at low frequencies, presenting a direct impact into the flight dynamic characteristics of the vehicle and controller design, as was seen in the Helios flight tests.[1]

The mission of the HALE aircraft is planned to be unmanned due to its "dull, dirty, or dangerous"[4] nature, i.e.,

> the attributes that make the use of unmanned preferable to manned aircraft ... [are] in the case of the dull, the better sustained alertness of machines over that of humans and, for the dirty and the dangerous, the lower political and human cost if the mission is lost, and greater probability that the mission will be successful. Lower downside risk and higher confidence in mission success are two strong motivators for continued expansion of unmanned aircraft systems.

For all the reasons stated, a better understanding of flight dynamics and control of these vehicles is required. This paper presents a control architecture specifically designed for the very flexible aircraft.

A. Previous Work

In 1914 Lawerence Sperry, son of Elmer Sperry, demonstrated his father's autopilot over Paris, by standing up in the cockpit of his airplane and having his mechanic walk out on the wing to create an external disturbance.[5] Sperry's invention was capable of maintaining pitch, roll, and heading angles.[6] This remarkable demonstration ushered in the use of the autopilot for a variety of aircraft and aircraft missions. Sperry's autopilot relied upon linear techniques and a relatively stiff biplane box type of construction. Since then control theory has evolved significantly. For an overview of aeroelastic control, Mukhopadhyay[7] has provided an excellent review paper of both analysis and control of aeroelastic structures over the past 100 years. He provides a summary of elastic theory, unsteady aerodynamics, control and highlights the future of nonlinear aeroelastic control. Recently researchers have looked at applying linear, robust control, and nonlinear techniques for aeroelastic control.

Modern linear control techniques such as Linear Quadratic Regulator (LQR) and Linear Quadratic Gaussian (LQG) observers have been applied by several researchers. Newman and Buttrill[8] have researched the longitudinal flight dynamics, longitudinal linear controller design, and sensor location for a high speed transport. Their aircraft modeling shows the importance of including elastic modes and sensor location when designing controllers for flexible aircraft and the difficulty in suppressing aeroelastic dynamic effects from the rigid body response of a flexible supersonic transport. Tuzcu[9] and Meirovitch and Tuzcu[10] have coupled nonlinear rigid body dynamics with linear structural dynamics. The formulation treats structural dynamics

as disturbance inputs to the rigid body dynamics. Results are presented for light weight transport aircraft using standard LQR and LQG control theory. Pedro and Bigg[11] have also applied traditional LQR and LQG techniques to a flexible aircraft. They developed a simulation to evaluate pilot ratings for an aeroelastic longitudinal aircraft model. Their approach looks only at the longitudinal dynamics with a Dryden gust model. Cesnik and Ortega-Morales[12] have utilized the geometrically exact beam formulation coupled with finite state aerodynamics and imbedded actuation to study and control flutter of a HALE type cantilevered wing. Their work focuses on the use of LQG observers to optimize sensor type, sensor placement, and actuation distribution. They have shown that a single strain gauge sensor, optimally placed, can provide the sensing necessary to control flutter of a high aspect ratio cantilevered wing.

Robust techniques using H_1, H_2, H_∞, and μ-synthesis have been studied by several researchers. Chavez and Schmidt[13] utilized linear structural modes to develop longitudinal controllers based upon μ-synthesis. Their work focuses on developing a systematic approach where robust controllers could be controlled without complete knowledge of the flexible system. They also present techniques for identifying structural modes of interest and methods of incorporating unsteady aerodynamics directly into the robust formulation without the necessity of building an aerodynamic state space model. Kron et. al.[14] have applied a reduced order H_∞ controller to a two-DOF lateral model of highly flexible transport aircraft. Their work focuses on characterizing model uncertainty when reducing the structural model. The uncertainty is then handled systematically through the development of a two-DOF H_∞ lateral controller. Finally numerical results are presented validating their method. Li and Agarwal[15] have also studied the use of a reduced order structural modeling to develop a linear robust controller using H_2 and H_∞ techniques for a high speed civil transport aircraft. They have shown, for that class of aircraft, the model reduction provides sufficient information for the linearized controller. Goman et. al.[16] have conducted a parametric study of various H_∞-based and traditional LQR/LQG controllers on a longitudinal elastic aircraft model. Their study shows similar controller designs between the two methods and improved robustness using the H_∞-based design.

Dardenne and Ferreres[17] have designed a lateral controller for highly flexible transport aircraft. The design assumes a linear time invariant (LTI) plant and uses a linear quadratic/programming procedure to design the controller utilizing frequency domain constraints. Their initial results have looked at reducing the wing bending effects on lateral motion. Patil[18] and Patil and Hodges[19] have also used minimization routines in designing a Static Output Feedback (SOF) controller used for flutter suppression of HALE type aircraft. The resulting controller is of a much lower order than LQR/LQG type controllers, but is valid only for a single operating condition. The authors comment that due to the simple design of the SOF controller, gain scheduling of different SOF controllers might be easily implemented.

Calise et. al.[20] have studied the use of output feedback (dynamic inversion) mixed with a neural network plant perturbation estimate to control a longitudinal flexible aircraft model. The process assumes a non-minimum phase (NMP) system with stable zero dynamics. They present initial results showing that their method could suppress structural mode interaction for a simplified longitudinal aircraft model. Krishnaswamy and Bugajski[21] have used dynamic inversion for studying control of rockets with fuel slosh. A key aspect of their study is the use of an underactuated system. They have developed an observer model for estimating the fuel slosh dynamics and show that the resulting controller can control the pitch dynamics of booster vehicle while damping fuel slosh dynamics. Finally, Gregory[22–25] has applied a "novel" Dynamic Inversion control technique for suppressing longitudinal motion due to linear aeroelastic effects of high speed transports. The variation in the Dynamic Inversion is the inclusion of pre-filters to move the structural modes further into the left half plane. Results show the ability to significantly improve ride control and longitudinal aircraft handling in the presence of longitudinal structural modes.

While most of the aeroelastic control work summarized here deals with different classes of aeroelastic effects than the very flexible HALE type aircraft, the control techniques, both linear and nonlinear, have potential relevance to trajectory control of very flexible aircraft.

B. Present Work

The objective of this paper is to present a control scheme for trajectory tracking of very flexible aircraft. It will be accomplished through a coupled 6-DOF vehicle dynamics with a modified version of the nonlinear strain-based structural formulation[26] for high-aspect-ratio lifting surfaces. The proposed control scheme is based loosely on human pilot operations. Simulations are presented both symmetric and asymmetric maneuvering and different aircraft loadings.

II. Theoretical Formulation

There are two fundamental approaches when developing a controller. The first is to treat the system of interest as a black box where the physics of the box are not known, but rather linearized transfer functions can be fit to input/output relationships. The second approach is to start with the known physics of the model and develop the controller. The later is used here and hence requires a basic understanding of the underlying governing differential equations.

The objective of the controller is to provide closed loop reference tracking of a body fixed reference frame, B, at point O, which in general is not the aircraft's center of mass, Figure 1, while including the effects of nonlinear aeroelasticity. The B reference can either be fixed inside a rigid section of the fuselage or more generally be attached to a node of an elastic fuselage. When the B frame is attached to a node of an elastic member, the y axis is chosen to be tangent to the undeformed longitudinal axis of the fuselage. The x axis is chosen to be positive out the right wing, such that for an undeformed wings level aircraft orientation, the $x-y$ plane is parallel to inertial frame G. The z axis is simply the cross product of the x and y axes. The tracking will consist of maintaining desired linear and angular velocities of the B reference frame. The

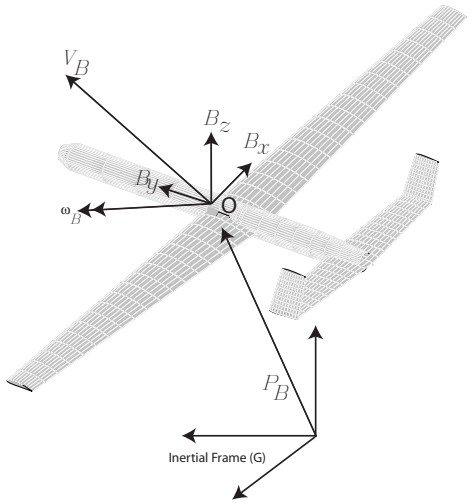

Figure 1. Basic body reference frame and vehicle coordinates

means for propagating the reference frame, B, forward in time is done by deriving and integrating a series of first-order differential equations of the form

$$\dot{x} = f(x, u) \tag{1}$$

where x represents the states of the reference frame, B, and u represents control surface and external inputs. Depending on the fidelity of the analysis, these first-order differential equations vary in their complexity from simple linear time invariant to nonlinear time varying differential equations. For the classic "rigid" body analysis,[27] the first-order differential equations take the form

$$\begin{aligned} \dot{v}_B &= f_{v_B}(v_B, \omega_B, \zeta, p_B, g_0^{'}, m, F_{ext}) \\ \dot{\omega}_B &= f_{\omega_B}(\omega_B, I_B, \zeta, p_B, M_{ext}) \\ \dot{\zeta} &= f_{\zeta}(\omega_B, \zeta) \\ \dot{p}_B &= f_{p_B}(\zeta, v_B) \end{aligned} \tag{2}$$

where the B reference frame linear and angular velocity variables are represented by v_B and ω_B; F_{ext} and M_{ext} are in general state dependent external forces and moments; m is the aircraft mass, and I_B is the aircraft's inertia matrix about the origin of the B reference frame. The orientation of the B reference frame is accomplished in a variety of ways from a minimum representation using three non-orthogonal Euler angles, to non-minimum four parameter quaternion representation, to a nine parameter set corresponding to the nine components of the set of unit vectors defining the triad at B. Reference 28 provides a summary of different methods used in the aerospace industry. In this paper, all three techniques are used to simplify the equations where necessary. In Eq. 2, ζ is the vector of four quaternion elements used to determine the orientation of the B reference frame and p_B is the inertial position of the B reference frame. The gravitational field effects are represented by $g_0^{'}$.

A. Summary of Governing Differential Equations

The rigid body formulation has three key assumptions which render invalid when dealing with very flexible vehicles: 1) inertia properties are constant or at best slowly time varying, 2) the coupling inertial force due to a rotating coordinate frame and relative velocity of flexible members is negligible, and 3) external forces and moments, F_{ext} and M_{ext}, which come from aerodynamic loading, are based upon a fixed aircraft geometry. In the rigid body case, Eq. 2 presents only inertial and external forces and moments. For the flexible aircraft a set of elastic EOM is also introduced, which in the context of this study results in

$$M\ddot{q} + C\dot{q} + Kq = R(q, \dot{q}, \lambda) \tag{3}$$

$$q = \left\{ \begin{array}{c} \epsilon \\ p_B \\ \Theta_B \end{array} \right\} \quad \dot{q} = \left\{ \begin{array}{c} \dot{\epsilon} \\ v_B \\ \omega_B \end{array} \right\} \quad \ddot{q} = \left\{ \begin{array}{c} \ddot{\epsilon} \\ \dot{v}_B \\ \dot{\omega}_B \end{array} \right\} \tag{4}$$

where M represents generalized mass properties, q is a set of generalized coordinates containing both strain, ϵ, associated with the flexible vehicle, and the inertial position, p_B, and an arbitrary orientation vector, Θ_B, of the B reference frame. The matrix C contains both structural damping and nonlinear terms associated with relative position and velocity terms associated with a rotating coordinate frame ($\omega_B \times v_B$, etc), K is the stiffness matrix, and $R(q, \dot{q}, \lambda)$ represents generalized forces (including aerodynamic forces) which are a function of the finite state inflow[29,30] velocities, λ. Coupling of the rigid body and flexible dynamics occurs through the dependency of M, C, and R. Typically the B reference frame linear and angular velocities are represented by

$$\beta = \left\{ \begin{array}{c} v_B \\ \omega_B \end{array} \right\} \tag{5}$$

The present work uses a constant strain-based formulation[26,31] which allows for airframe nonlinear geometric deformation and accounts for geometry-dependent inertia properties of the aircraft.

To develop the nonlinear governing differential equations for slender elastic structures, a systematic approach is used where the rigid body and elastic EOM are developed about the B reference frame. The differential equations for the orientation and displacement of the B reference frame are appended based upon a four state quaternion representation. Unsteady aerodynamic modeling is included and, if required, algebraic equations for absolute or relative constraints are appended (example of which is a joined wing aircraft as shown in Figure 2, where relative constraints are needed at the joint of the two wings).

The derivation of the EOM is based upon the principle of virtual work. The method accounts for the virtual work associated with the B reference system, flexible aircraft slender (beam) structural members, and rigid bodies attached to the flexible structures. The virtual work of a beam and rigid bodies attached to a beam are initially written in terms of dependent displacement vectors. Then the kinematic relationship between beam dependent position vectors and the associated strains is developed. The components of virtual work are summed and the resulting set of equations are transformed from a set of dependent position vectors and a nonminimum set of B reference frame components to an independent set of strain variables and body linear and angular velocities.

The final virtual work expression, which includes both B reference frame and flexible body contributions,

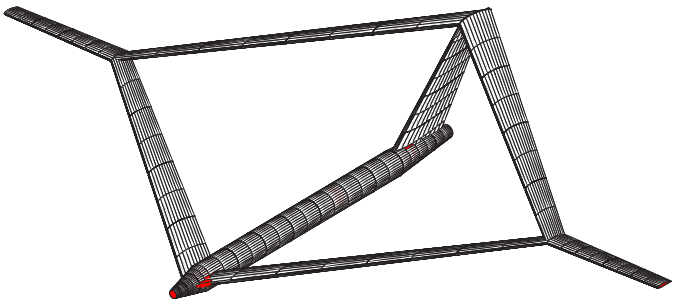

Figure 2. Joined wing aircraft concept

is written

$$\delta W = \left[\begin{array}{cc} \delta\epsilon^T & \delta b^T \end{array} \right]^T \left(- \left[\begin{array}{cc} M_{FF} & M_{FB} \\ M_{BF} & M_{BB} \end{array} \right] \left[\begin{array}{c} \ddot{\epsilon} \\ \dot{\beta} \end{array} \right] - \left[\begin{array}{cc} C_{FF} & C_{FB} \\ C_{BF} & C_{BB} \end{array} \right] \left[\begin{array}{c} \dot{\epsilon} \\ \beta \end{array} \right] + \right.$$
$$\left. - \left[\begin{array}{cc} K_{FF} & K_{FB} \\ K_{BF} & K_{BB} \end{array} \right] \left[\begin{array}{c} \epsilon \\ b \end{array} \right] + R \right), \tag{6}$$

where the generalized mass and damping matrices are given by

$$\begin{array}{ll} M_{FF} = J_{h\epsilon}^T M_G J_{h\epsilon} & M_{FB} = J_{h\epsilon}^T M_G J_{hb} \\ M_{BF} = J_{hb}^T M_G J_{h\epsilon} & M_{BB} = J_{hb}^T M_G J_{hb} + M_B \\ C_{FF} = J_{h\epsilon}^T M_G \dot{J}_{h\epsilon} + C_G & C_{FB} = J_{h\epsilon}^T M_G H_{hb} + 2 J_{h\epsilon}^T M_G H_{h\dot{\epsilon}\dot{\beta}} \\ C_{BF} = J_{hb}^T M_G \dot{J}_{h\epsilon} & C_{BB} = J_{hb}^T M_G H_{hb} + 2 J_{hb}^T M_G H_{h\dot{\epsilon}\dot{\beta}} + C_B \\ K_{FF} = K_G & K_{FB} = 0 \\ K_{BF} = 0 & K_{BB} = 0 \end{array} \tag{7}$$

and M_G, C_G, and K_G are the assembled flexible-element generalized mass, damping, and stiffness matrices, respectively. The matrices M_B and C_B represent the mass and damping matrices associated with the B frame rigid element portion as described in Refs. 32, 33. The jacobian matrices, $J_{h\epsilon}$ and J_{hb}, provide relationships between flexible position and orientation vectors and the independent coordinates of strain, ϵ, and B reference frame linear and angular velocities, β. Additional matrices, H_{hb} and $H_{h\dot{\epsilon}\dot{\beta}}$, capture the dynamics of a rotating coordinate frame. Complete details of the derivation are provided in Refs 32, 33. Note the traditional aircraft rigid body EOM can be recovered from the flexible EOM, Eq. 6, by assuming the elastic DOF are constant. This is described in detail in Ref. 33. The resultant force vector R is

$$R = \left\{ \begin{array}{c} R_F \\ R_B \end{array} \right\} = \left[\begin{array}{c} K_{FF} \\ K_{BF} \end{array} \right] \epsilon_{initial} + \left[\begin{array}{c} B_{gF} \\ B_{gB} \end{array} \right] g^B + \left[\begin{array}{c} B^F_{dst_F} \\ B^F_{dst_B} \end{array} \right] F^{dst} + \left[\begin{array}{c} B^M_{dst_F} \\ B^M_{dst_B} \end{array} \right] M^{dst} +$$
$$+ \left[\begin{array}{c} B^F_{p_F} \\ B^F_{p_B} \end{array} \right] F^{pt} + \left[\begin{array}{c} B^M_{p_F} \\ B^M_{p_B} \end{array} \right] M^{pt}$$

where $\epsilon_{initial}$ is an initial strain vector, g^B is the body-frame-B resolved gravity vector, and F^{dst}, M^{dst}, F^{pt}, and M^{pt}, are body resolved distributed and point forces and moments. The aerodynamic forces and moments,

F^{aero} and M^{aero}, which are functions of control surface inputs, u, are included in F^{dst} and M^{dst}. The influence matrices are derived as[31]

$$B^F_{dst_F} = J^T_{p\epsilon} B_F \qquad B^F_{dst_B} = J^T_{p\beta} B_F \tag{8}$$

$$B^M_{dst_F} = J^T_{\theta\epsilon} B_M \qquad B^M_{dst_B} = J^T_{\theta\beta} B_M \tag{9}$$

$$B^F_{p_F} = J^T_{p\epsilon} \qquad B^F_{p_B} = J^T_{p\beta} \tag{10}$$

$$B^M_{p_F} = J^T_{\theta\epsilon} \qquad B^M_{p_B} = J^T_{\theta\beta} \tag{11}$$

where the matrices B_F and B_M are constant matrices defined by an elastic element's undeformed length. For more details please see Ref 31. For simplicity the initial strain, $\epsilon_{initial}$ and point moments, M^{pt} will be assumed to be zero. The finite strain formulation[29,30] for aerodynamic forces and moments is linear in the discrete trailing edge surface deflections. These assumptions and formulations combined with a point force representing a simplistic engine model allow the generalized force to be expressed as

$$R = [B_g]\, g^B + \left[B^F_{dst}\right] F^{aero} + \left[B^M_{dst}\right] M^{aero} + \left[B^F_{dst}\right] \frac{\partial F^{aero}}{\partial u_{flap}} u_{flap} + \left[B^F_p\right] u_{thrust} \tag{12}$$

For additional details see Ref. 26. From the Principle of Virtual Work, Eq. 6 yields

$$\begin{bmatrix} M_{FF} & M_{FB} \\ M_{BF} & M_{BB} \end{bmatrix} \begin{bmatrix} \ddot{\epsilon} \\ \dot{\beta} \end{bmatrix} + \begin{bmatrix} C_{FF} & C_{FB} \\ C_{BF} & C_{BB} \end{bmatrix} \begin{bmatrix} \dot{\epsilon} \\ \beta \end{bmatrix} + \begin{bmatrix} K_{FF} & K_{FB} \\ K_{BF} & K_{BB} \end{bmatrix} \begin{bmatrix} \epsilon \\ b \end{bmatrix} = \begin{Bmatrix} R_F \\ R_B \end{Bmatrix} \tag{13}$$

This set of equations are the ones given in a compact form by Eq. 3. Note that $M = M(\epsilon)$ and $C = C(\epsilon, \dot{\epsilon}, \beta)$, and K the generalized stiffness. All the other nonlinearities are contained in the generalized force, R. When the EOM, Eq. 13, are augmented with the B reference frame orientation, position, and unsteady aerodynamics, the complete set of governing differential equations is

$$\begin{aligned} M_{FF}\ddot{\epsilon} &= -M_{FB}\dot{\beta} - C_{FF}\dot{\epsilon} - C_{FB}\beta - K_{FF}\epsilon + R_F \\ M_{BB}\dot{\beta} &= -M_{BF}\ddot{\epsilon} - C_{BB}\beta - C_{BF}\dot{\epsilon} + R_B \\ \dot{\zeta} &= -\frac{1}{2}\Omega_\zeta \zeta \\ \dot{p}_B &= \begin{bmatrix} C^{BG} & 0 \end{bmatrix} \beta \\ \dot{\lambda} &= F_1\ddot{q} + F_2\dot{q} + F_3\lambda \end{aligned} \tag{14}$$

where ζ is a vector of four quaternion parameters used for the orientation of the B reference frame, $\dot{p}_B$ is the the inertial position vector of the B reference frame (Figure 1), C^{BG} is a transformation matrix between a B reference frame vector and an inertial (G) vector, λ is a set of unsteady aerodynamic inflow velocities with associated differential equation matrices F_1 through F_3. For complete details please see Refs. 32, 33.

B. Trimming the Aircraft

Trimming is performed for both zero thrust and thrust required for 1-g level flight based upon techniques outlined in Refs. 27 and 34. A cost function is defined as

$$J = f^T \cdot f \tag{15}$$

where for the zero thrust or gliding cases,

$$f = \begin{Bmatrix} \text{pitching moment about the origin of } B \text{ frame} \\ \text{lift} - \text{weight} \end{Bmatrix} \tag{16}$$

For the case of 1-g level flight, the longitudinal B reference frame linear and angular accelerations are used, such that

$$f = \begin{Bmatrix} \dot{v}_{B_y} \\ \dot{v}_{B_z} \\ \dot{\omega}_x \end{Bmatrix} \tag{17}$$

The cost function J is then minimized over the solution space using the elevator deflection angle, δ_e, the body angle of attack, α, and thrust, δ_t. A simple numerical Newton-Raphson method is used to find the local minimum of the search variable, i.e.,

$$\Delta\mathcal{S}_k = -\left[\frac{\partial f}{\partial \mathcal{S}}\right]_k^{-1} f_k \tag{18}$$

where

$$\mathcal{S}_k = \left\{ \begin{array}{c} \delta_e \\ \alpha \\ \delta_t \end{array} \right\}_k \tag{19}$$

The search variable, $\mathcal{S}$, is updated by

$$\mathcal{S}_{k+1} = \mathcal{S}_k + \Delta\mathcal{S} \tag{20}$$

and f_{k+1} and $\left[\frac{\partial f}{\partial \mathcal{S}}\right]_{k+1}^{-1}$ are recomputed using $\mathcal{S}_{k+1}$. The process continues until the cost function J reduces to some prescribed tolerance. To prevent divergence of the solution, $\mathcal{S}_{k+1}$ is checked at each iteration step and kept within a prescribed set of bounds. The Jacobian

$$J_f = \frac{\partial f}{\partial \mathcal{S}} \tag{21}$$

is computed numerically through finite differences. The entire procedure is outlined in Figure 3.

C. Solution of EOM

To solve the nonlinear differential equations, Eq. 14, a high frequency dissipative time stepping approach was implemented. A Modified Newmark Method was used and is described in Ref. 35. The Modified Newmark Method was selected based upon its ability to accurately integrate large systems of equations including ones with repeated eigenvalues, its relative ease of implementation with the current EOM modeling, and the derivation of both a first and second order method.[36,37]

III. Trajectory Control of Very Flexible Aircraft

A. Challenges for Trajectory Control of Very Flexible Aircraft

Due to the nature of the very flexible aircraft construction, the wings will typically have a lower stiffness than the fuselage, generating stronger coupling of the rigid body and structural motion in the lateral axis than in the longitudinal one. This creates a variety of challenges to be overcome by controllers. The first is the requirement of an integrated controller which handles flexibility as well as rigid body motion. Typically the first wing bending mode of this class of aircraft is less than 10 rad/s, creating direct interaction with classic lateral and longitudinal rigid body aircraft modes (spiral, roll, dutch roll, phugoid). The second major challenge is a time delay between control inputs and B reference frame movement due to the flexibility of the aircraft. This time delay creates a non-minimum phase (NMP) system when the governing differential equations are linearized. The third major challenge is the introduction of additional NMP behavior due to adverse yaw from aileron inputs. The adverse yaw problem may be avoided through the use of spoilers for roll control, but that is not addressed in this work. The fourth challenge is the location of the linearized structural eigenvalues near the imaginary axis. And finally the generalized mass and damping matrices are state dependent.

B. Requirements and Assumptions for Trajectory Control of Very Flexible Aircraft

Before designing any controller, a set of performance objectives should be established. Currently, despite operational requirements,[4] there are no published performance specification requirements for very flexible aircraft either from the military, civilian government, or industry authorities. Given this void, it is worthwhile to refer back to the piloted aircraft military standards, MIL-STD-1797A .[38] While very flexible aircraft do not have the safety requirements inherent in piloted aircraft, minimal control performance requirements are necessary for both manned and unmanned aircraft to complete the various missions and potentially fly in

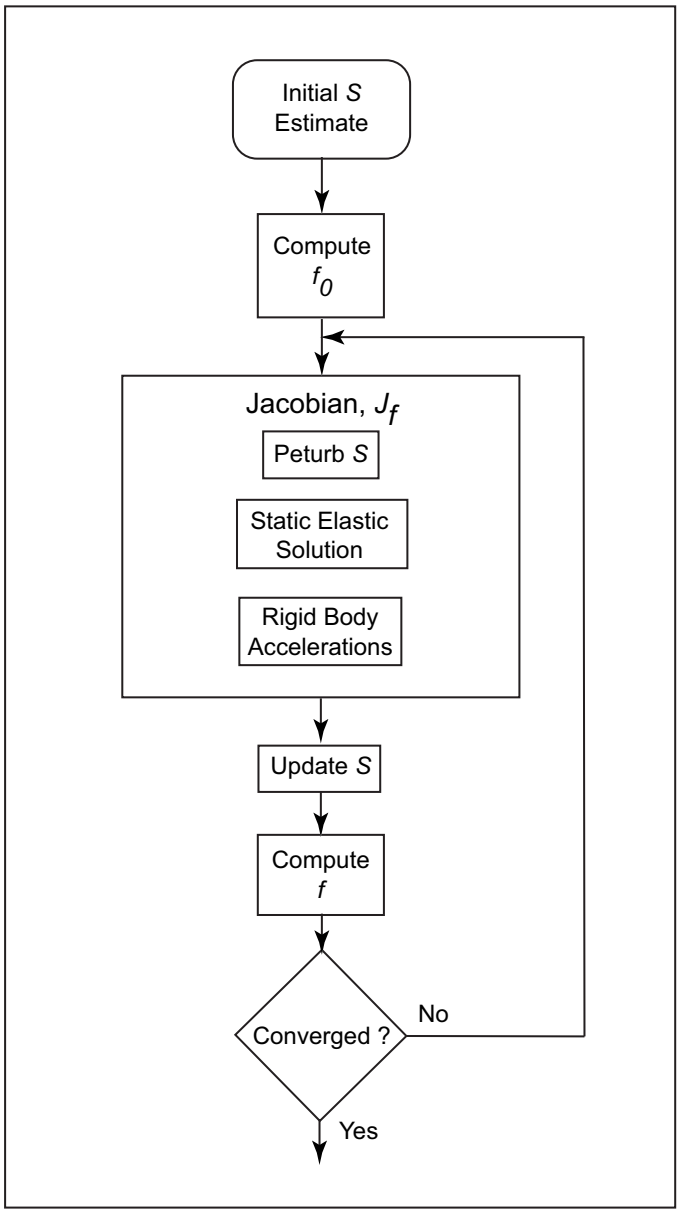

Figure 3. Flow for Trim Solution

the National Airspace System. For classification purposes, a very flexible vehicle will be considered a large land based transport type aircraft, Class III-L, as in Table 1. From MIL-STD-1797A , Table 2 summarizes

Table 1. Aircraft classes as defined in MIL-STD-1797A

Class	Type of Aicraft	Example
I	Small Light Aircraft	Primary Trainer, Light Utility
II	Medium Weight, Low-to-medium maneuverability	Search and Rescue, ISR
III	Large, Heavy, Low-to-medium maneuverability	Heavy Transport, ISR
IV	High Maneuverability Aircraft	Fighter, Attack
Note: a -L stands for land based and a -C for carrier based		

the desired roll requirements for Level 2 flying qualities (Table 3) during take-off, climb, loiter, and landing flight conditions. Furthermore, the maximum bank angle required shall be determined by the bank angle

Table 2. Final roll performance objectives for very flexible aircraft

Flight Phase	Bank Angle Change/ Seconds to achieve	Roll Mode time constant
Climb and Loiter -B*	30°/3.9 s	3.0 s
Take-off and Landing -C*	30°/4.0 s	3.0 s
Note: * is the letter designator from MIL-STD-1797A for the particular flight phase		

Table 3. Qualitative degrees of suitability and levels as defined in MIL-STD-1797A

Level	Description
1 - Satisfactory	Flying Qualities clearly adequate for the mission Flight Phase
2 - Acceptable	Flying Qualities adequate to accomplish the mission Flight Phase
3 - Controllable	Flying Qualities such that the aircraft can be controlled in the context of the mission Flight Phase ... workload is excessive or mission effectiveness is inadequate

required to make a standard two-minute turn (turn rate of $3^\circ \frac{1}{s}$ or 0.05236 $\frac{rad}{s}$). Since MIL-STD-1797A does not provide specific guidance for climb rates, a maximum climb rate of 2000 $\frac{ft}{min}$ ($10.16 \frac{m}{s}$) at sea-level at maximum gross weight shall be used. This rate is based upon reasonable climb rates of aircraft similar in size and weights.

Three basic maneuvers will be used to study controller performance. The first maneuver is a wings-level altitude change. The second maneuver is a steady level turn starting from a zero bank angle. And the third maneuver is climbing turn.

Finally the assumption will be made that the aircraft will be flying well below any divergence, flutter, or limit cycle oscillation boundaries. While this assumption is restrictive for an aircraft dominated by aeroelastic effects, it is an important first step in the development of controllers for performing basic aircraft maneuvering. Future research should focus on extending the controller(s) beyond aeroelastic boundaries.

C. Development of a Control Architecture for Very Flexible Aircraft

As discussed in Section III.A, very flexible aircraft, and particularly HALE ones, present unique challenges to the design of a controller. This section details the specifics of a proposed very flexible aircraft controller.

1. *Traditional Controller Design Difficulty*

Traditional methods of modern aircraft control[6,27,39] have relied upon the state vector

$$x = \begin{bmatrix} v_{B_x} & v_{B_y} & v_{B_z} & \omega_{B_x} & \omega_{B_y} & \omega_{B_z} & \Phi & \Theta & \Psi & p_{B_x} & p_{B_y} & p_{B_z} \end{bmatrix}^T \tag{22}$$

or variations of x, where the B reference frame linear and angular velocities are v_B and ω_B, the classic Euler angles of roll (positive right wing down), pitch (positive nose up), and yaw (positive nose right) are given by Φ, Θ, and Ψ respectively, and the inertial position is given by p_B. Linearizing the rigid body governing differential equations about this state vector, and determining a constant gain matrix, K, has been shown in numerous papers and books to yield satisfactory results when applied to nonlinear flight dynamic models. However, the current problem with additional aeroelastic effects has rendered this to be ineffective for trajectory control. In the process of developing a stabilizing controller architecture for very flexible aircraft, traditional controller designs were initially applied to a statically deformed rigid aircraft model. This controler architecture was shown to have difficulties in providing closed loop stable trajectory tracking.[33]

2. *A Heuristic Approach Mimicking a Human Pilot*

Due to the difficulty in finding a stable controller for the rigid body using traditional techniques, the method was not attempted with additional elastic states. A method of decoupling the linear and nonlinear effects of the aircraft response was designed based loosely upon aircraft pilot training. A well trained human pilot has been taught to command flight path angle, γ, bank angle, μ, and their rates, $\dot{\gamma}$ and $\dot{\mu}$, when changing altitude or heading Ψ, through a fast- (inner) and slow- (outer) loop process. The fast-loop consists of commanding pitch rate, pitch angle, roll rate, and sideslip angle. These changes are commanded by the pilot typically through the use of four controls: elevator (δ_e), aileron (δ_a), rudder (δ_r), and throttle (δ_t). Once an angle and its rate have been satisfactory set, the pilot then performs a slow-loop (outer-loop) function of cross checking altitude, rate of climb, and other states. Heffley et. al.[40] have described this type of inner- and outer-loop control as an implicit inner-loop and explicit outer-loop tracking task. Additionally for level turns, altitude changes, and landing flair maneuvers, Heffley and Schulman[41] have provided pilot models for outer-loop control.

In similar fashion, this work proposes building a stable inner-loop, utilizing both linear and nonlinear theory, where the states are the linear and angular B reference frame velocities, β, Eq. 5, and augmented error states. The outer-loop or slow-loop is then controlled through a nonlinear transformation and traditional proportional, integral, derivative (PID) control techniques.[42] Conceptually the entire system is shown in Figure 4. In the figure β_0 are the initial trimmed B reference frame linear and angular velocities. For the outer-loop a commanded B reference frame velocity, β_{com} and differences are generated

$$\Delta\beta_{com} = \beta_{com} - \beta \tag{23}$$

and used to excite inner-loop integrator error states. For the inner-loop the difference in β

$$\Delta\beta = \beta - \beta_0 \tag{24}$$

is required to generate differences in the control vector from the initial control deflections, u_0, such that

$$u = u_0 + \Delta u \tag{25}$$

and Δu is a function of the gain matrix, K, and the augmented error states, e

$$\Delta u = K\left(\Delta\beta, e\right) \tag{26}$$

Also the subscripts *des* and *com* are the desired and commanded values.

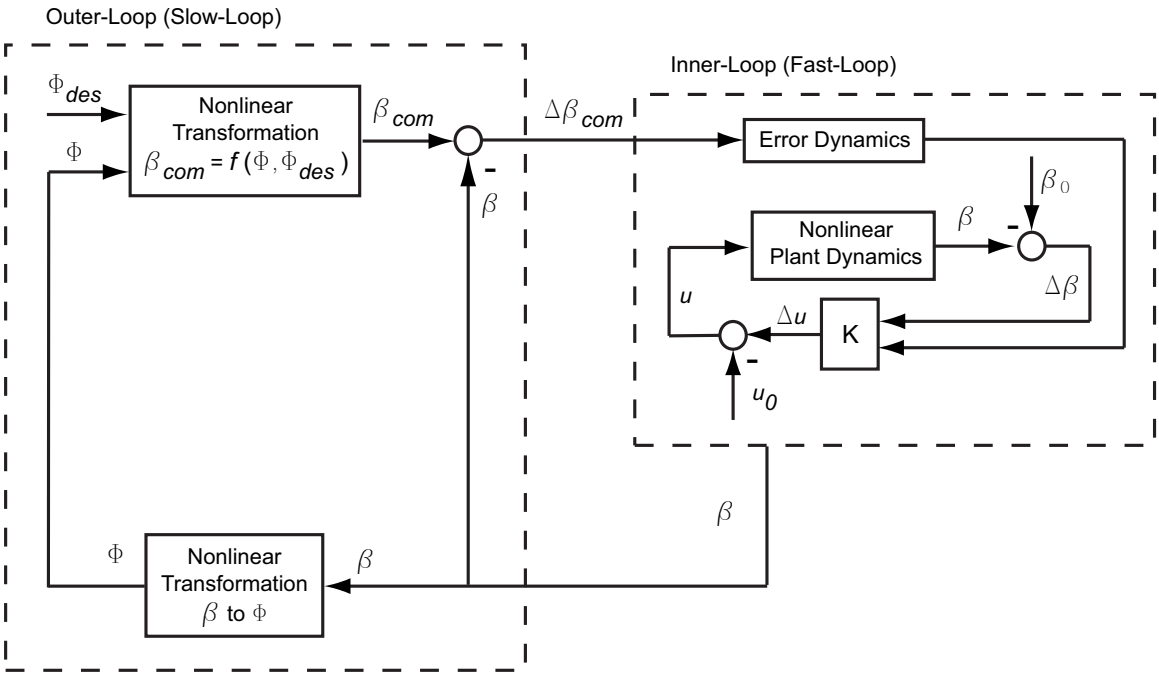

Figure 4. Controller Concept Mimicking a Human Pilot

3. Nonlinear Transformation from Flight Path and Bank Angles to Body Velocities

The classic rigid body aircraft kinematic equations used for the nonlinear transformation are[27,39,43]

$$V = \sqrt{u^2 + v^2 + w^2} \tag{27}$$

$$\beta_s = \sin^{-1}(v/V) \tag{28}$$

$$\gamma = \sin^{-1}\left((\cos\alpha\sin\Theta - \sin\alpha\cos\Theta\cos\Phi)\cos\beta_s - \cos\Theta\sin\Phi\sin\beta_s\right) \tag{29}$$

$$\mu = \sin^{-1}\left(\frac{\cos\Theta\sin\Phi\cos\beta_s + (\cos\alpha\sin\Theta - \sin\alpha\cos\Theta\cos\Phi)\sin\beta_s}{\cos\gamma}\right) \tag{30}$$

$$\dot{\Phi} = P + \tan\Theta\,(Q\sin\Phi + R\cos\Phi) \tag{31}$$

$$\dot{\Theta} = Q\cos\Phi - R\sin\Phi \tag{32}$$

where V is the total airspeed and the classic aircraft longitudinal, lateral, and vertical velocity components are u positive out the nose, v positive out the right wing, and w positive down. Further γ is the flight path elevation angle, α is the aircraft angle of attack, μ the flight path bank angle, and β_s the sideslip angle. The classic aircraft angular rates are roll rate, P, pitch rate, Q, and yaw rate, R. The dynamic equations of interest are

$$L = \frac{1}{2}\rho V^2 S C_{L_\alpha}\alpha \tag{33}$$

$$\dot{v} = -Ru + Pw + g_0^{'}\sin\Phi\cos\Theta + \frac{F_y}{m} \tag{34}$$

where L is the aircraft lift, ρ is the atmospheric density, S is the surface area of the wing, C_{L_α} is the equivalent aircraft lift curve slope, $g_0^{'}$ is the magnitude of the gravity vector, F_y is the lateral force due to aerodynamic and control inputs, and m is the aircraft mass. Equation 33 is a steady state lift approximation and will be used to develop an angle-of-attack, α, dynamic relationship. Equation 34 is the rigid body lateral acceleration EOM and will be used to develop relationships for the B reference frame angular velocities. The

angle of attack and sideslip are related to the longitudinal velocites as

$$\left\{ \begin{array}{c} u \\ v \\ w \end{array} \right\} = \left\{ \begin{array}{c} V\cos(\alpha)\cos(\beta_s) \\ V\sin(\beta_s) \\ V\sin(\alpha)\cos(\beta_s) \end{array} \right\} \tag{35}$$

such that the angle of attack may be written as

$$\alpha = \tan^{-1}(w/u) \tag{36}$$

Before Eqs. 27 - 36 can be used in the current formulation, transformations of the linear and angular body velocities and quaternion to classic Euler angles are presented. For the linear and angular velocities the relationships are

$$\left\{ \begin{array}{c} v_{B_x} \\ v_{B_y} \\ v_{B_z} \end{array} \right\} = \left[\begin{array}{ccc} 0 & 1 & 0 \\ 1 & 0 & 0 \\ 0 & 0 & -1 \end{array} \right] \left\{ \begin{array}{c} u \\ v \\ w \end{array} \right\} \tag{37}$$

and

$$\left\{ \begin{array}{c} \omega_{B_x} \\ \omega_{B_y} \\ \omega_{B_z} \end{array} \right\} = \left[\begin{array}{ccc} 0 & 1 & 0 \\ 1 & 0 & 0 \\ 0 & 0 & -1 \end{array} \right] \left\{ \begin{array}{c} P \\ Q \\ R \end{array} \right\} \tag{38}$$

To develop the quaternion relationship, first the body, B, to inertial, G, rotation matrix in terms of the Euler angles is found as

$$C^{GB} = \left[\begin{array}{ccc} (c\Phi\ c\Psi + s\Phi\ s\Theta\ s\Psi) & (-c\Phi\ s\Psi + s\Phi\ s\Theta\ c\Psi) & -s\Phi\ c\Theta \\ c\Theta\ s\Psi & c\Theta\ c\Psi & s\Theta \\ (s\Phi\ c\Psi - c\Phi\ s\Theta\ s\Psi) & -(s\Phi\ s\Psi + c\Phi\ s\Theta\ c\Psi) & c\Phi\ c\Theta \end{array} \right] \tag{39}$$

where the shorthand $\cos\Phi \equiv c\Phi$ and $\sin\Phi \equiv s\Phi$ is used. The Euler angles of interest have the following relationship to the quaternions[33]

$$\sin\Theta = 2(\zeta_2\zeta_3 + \zeta_0\zeta_1) \tag{40}$$

$$\cos\Theta\cos\Phi = \zeta_0^2 - \zeta_1^2 - \zeta_2^2 + \zeta_3^2 \tag{41}$$

$$\cos\Theta\sin\Phi = 2(-\zeta_1\zeta_3 + \zeta_0\zeta_2) \tag{42}$$

To perform the transformation from given inputs of flight path angle and bank angle to desired body velocities, the following assumptions are made:

1. Angle of side-slip, β_s, is zero;
2. The Euler bank angle, Φ will be used in place of bank angle μ;
3. Total velocity, V, is prescribed and typically assumed constant;
4. Angle of attack, α, is proportional to $\cos\Phi$;
5. Lateral side forces are only a function of cross coupling of linear and angular velocities and gravity component due to Euler bank and pitch angle, and lateral velocity is constant.

While zero side slip, assumption 1, is typically a requirement of manned aircraft for comfort reasons, it is also desired to minimize coupling of the lateral and longitudinal aircraft motion. Assumption 2 is justified by applying small angle assumptions to γ, Euler pitch angle, Θ, and angle of attack, α. Using these assumptions and Eq. 29

$$\mu \approx \Phi \tag{43}$$

Further, if a navigational loop is wrapped around the architecture described in Figure 4, the Euler roll angle would be convenient as an input. Assumption 3 is made to simplify the resulting nonlinear transformation equations. Assumption 4 has two significant effects. The first is unsteady aerodynamic effects presented

in Ref. 32, are neglected. This is done because one of the goals of this work is to development an initial control architecture for very flexible aircraft, without consideration of aeroelastic boundaries. Additionally the controller is designed to maintain aircraft velocities well below these aeroelastic boundaries, preventing destabilization of the controller through unmodeled dynamics (within the controller). The second significant effect of assumption 4 is an increase in angle-of-attack to generate additional lift for a wings-level climb is not considered. This is reasonable approximation utilized in most rigid body aircraft performance equations[43] where

$$\text{Rate of Climb} = \frac{\text{Excess Thrust}}{\text{Weight}} \tag{44}$$

Assumption 4 is derived from the steady level-turn performance equation[43]

$$n_{load} = \frac{1}{\cos\Phi} \tag{45}$$

where the load factor, n_{load}, is the non-dimensionalized acceleration of gravity. Assuming linear three dimensional lift theory and a level turn

$$L_\Phi = n_{load} L_{\Phi=0} \tag{46}$$

Using Eq. 33 in Eq. 46, it can be shown that

$$\alpha_\Phi = \frac{1}{\cos\Phi}\alpha_0 \tag{47}$$

where α_0 is the angle of attack corresponding to a wings level at steady level flight. Finally assumption 5, which simplifies the lateral EOM, Eq. 34, provides one of three resulting equations used to determine the B reference frame angular velocities.

Using Eqs. 27 - 47 and the five assumptions, the resulting set of equations are:

- angle of attack relationships:

$$\begin{aligned} \alpha &= \frac{1}{\cos\Phi}\alpha_0 && (48)\\ \dot{\alpha} &= \tan\Phi\sec\Phi\ \alpha_0\ \dot{\Phi} && (49) \end{aligned}$$

- linear body velocity relationships:

$$\begin{aligned} v_{B_z} &= -V\sin\alpha && (50)\\ \dot{v}_{B_z} &= -V\cos\alpha\ \dot{\alpha} && (51)\\ v_{B_y} &= \sqrt{V^2 - v_{B_z}^2} && (52)\\ \dot{v}_{B_y} &= -\frac{v_{B_z}\dot{v}_{B_z}}{v_{B_y}} && (53) \end{aligned}$$

- flight path angle, Euler pitch angle, and angle of attack relationships:

$$\begin{aligned} \sin\gamma &= \cos\alpha\sin\Theta - \cos\Phi\sin\alpha\cos\Theta && (54)\\ \dot{\Theta} &= \frac{\cos\gamma\dot{\gamma} + (\sin\alpha\sin\Theta + \cos\Phi\cos\alpha\cos\Theta)\,\dot{\alpha}}{\cos\alpha\cos\Theta + \cos\Phi\sin\alpha\sin\Theta} + \\ &\quad -\frac{\sin\Phi\sin\alpha\cos\Theta\ \dot{\Phi}}{\cos\alpha\cos\Theta + \cos\Phi\sin\alpha\sin\Theta} && (55) \end{aligned}$$

- body angular velocity relationships.

$$\begin{aligned} \dot{\Phi} &= (\tan\Theta\sin\Phi)\,\omega_{B_x} + \omega_{B_y} - (\tan\Theta\cos\Phi)\,\omega_{B_z} && (56)\\ g_0^{'}\sin\Phi\cos\Theta &= v_{B_z}\ \omega_{B_y} - v_{B_y}\ \omega_{B_z} && (57)\\ \dot{\Theta} &= \cos\Phi\ \omega_{B_x} + \sin\Phi\ \omega_{B_z} && (58) \end{aligned}$$

Given the flight path angle and rate, γ and $\dot{\gamma}$, and the Euler roll angle and rate, Φ and $\dot{\Phi}$, Eqs. 48 - 58 are used to solve for the commaned B reference velocities, β_{com}.

To close the outer-loop of Figure 4, the actual flight path angle, γ, Euler bank angle, Φ, and their rates, $\dot{\gamma}$ and $\dot{\Phi}$ are determined. Differences are then found

$$\begin{aligned} \Delta\gamma &= \gamma - \gamma_{des} \\ \Delta\dot{\gamma} &= \dot{\gamma} - \dot{\gamma}_{des} \\ \Delta\Phi &= \Phi - \Phi_{des} \\ \Delta\dot{\Phi} &= \dot{\Phi} - \dot{\Phi}_{des} \end{aligned} \tag{59}$$

The commanded flight path elevation angle and Euler roll angle are computed using a traditional linear technique of proportional, integral, derivative (PID) control

$$\begin{aligned} \gamma_{com} &= \gamma_{des} + \Delta\gamma_{com} \\ \dot{\gamma}_{com} &= \dot{\gamma}_{des} + \Delta\dot{\gamma}_{com} \\ \Phi_{com} &= \Phi_{des} + \Delta\Phi_{com} \\ \dot{\Phi}_{com} &= \dot{\Phi}_{des} + \Delta\dot{\Phi}_{com} \end{aligned} \tag{60}$$

where

$$\begin{aligned} \Delta\gamma_{com} &= k_\gamma \Delta\gamma + k_{I\gamma} \int_0^t (\Delta\gamma)\, d\tau + k_{II\gamma} \int_0^t \left(\int_0^t (\Delta\gamma)\, d\tau \right) d\tau + k_{d\gamma} \Delta\dot{\gamma} \\ \Delta\dot{\gamma}_{com} &= k_{\dot{\gamma}} \Delta\dot{\gamma} + k_{I\dot{\gamma}} \Delta\gamma + k_{II\dot{\gamma}} \int_0^t (\Delta\gamma)\, d\tau + k_{III\dot{\gamma}} \int_0^t \left(\int_0^t (\Delta\gamma)\, d\tau \right) d\tau \\ \Delta\Phi_{com} &= k_\Phi \Delta\Phi + k_{I\Phi} \int_0^t (\Delta\Phi)\, d\tau + k_{d\Phi} \Delta\dot{\Phi} \\ \Delta\dot{\Phi}_{com} &= k_{\dot{\Phi}} \Delta\dot{\Phi} + k_{I\dot{\Phi}} \Delta\Phi + k_{II\dot{\Phi}} \int_0^t (\Delta\Phi)\, d\tau \end{aligned} \tag{61}$$

The outer-loop feedback gains, k_γ, $k_{I\gamma}$, etc, of Eq. 61 are initially determined using the SISO heuristic guidelines of Ziegler and Nichols[44,45] where

$$u = k_c e + k_I \int e\ dt + k_d \dot{e} \tag{62}$$

For PID and PI controllers, Ziegler and Nichols recommend values are given in Table 4, where k_u is the closed loop gain required to make the system marginally stable and t_u is the corresponding period between oscillations. The gains are then adjusted to meet desired performance. Due to the potential instability of

Table 4. Ziegler and Nichols[44,45] PID and PI tuning parameters

	PID	PI
Proportional Gain	$k_c = 0.6k_u$	$k_c = 0.45k_u$
Integral Gain	$k_I = \frac{k_c}{0.5t_u}$	$k_I = \frac{k_c}{0.85t_u}$
Derivative Gain	$k_d = \frac{1}{8}k_c t_u$	

integral feedback,[42] the additional integral gains ($k_{II\gamma}$, $k_{II\dot{\gamma}}$, $k_{III\dot{\gamma}}$, etc.) are chosen to be at least an order or more of magnitude less than the first integral gains ($k_{I\gamma}$, $k_{I\dot{\gamma}}$, etc.).

D. Modification of Proposed Control Architecture to a Flexible Vehicle

This section presents a method for extending the control architecture previously introduced to a flexible aircraft. First a separation of the lateral and longitudinal motion is presented. Then control techniques are applied to the lateral and longitudinal motion separately. Finally coupling between the lateral and longitudinal motion is shown to be handled in an outer-loop strategy.

Section III.C outlined a control strategy for very flexible aircraft. The philosophy of this approach is to provide a systematic method where the dominant coupling of lateral and longitudinal motion is handled in a slower outer-loop, and B reference frame linear and angular velocities are handled in a faster inner-loop. The six states (linear and angular B reference frame velocities) of the inner-loop are typically easily separated into longitudinal and lateral motion with corresponding control effectors. This allows individual control schemes to be applied to each set of the inner-loop dynamics (longitudinal and lateral). The outer loop controls the required longitudinal and lateral motion necessary for trajectories where this motion is coupled, i.e. steady level turns and climbing turns. Additionally the outer-loop handles coupling of the lateral and longitudinal motion due to gravitational effects. While this idea is not new and has been applied to high-angle-of-attack flight,[46–48] it typically has not been applied to "low- to moderate-angle-of-attack flight regimes".[47] This is due largely to traditional aircraft control design assuming relatively small to moderate amounts of nonlinear cross coupling. With very flexible aircraft, the large potential movement of the *cm* from the origin of the B reference frame can create a significant nonlinear coupling.

1. *Separation of Lateral and Longitudinal Motion*

As shown by Shearer and Cesnik,[32,33] for this class of vehicles with relatively stiff fuselages, longitudinal motion does not appear to be significantly affected by wing flexibility. So it is assumed that wing flexibility is a secondary and minimal contribution to aircraft longitudinal motion. Using this assumption and the previous assumptions of Section III.C.3, a separation between longitudinal and lateral/elastic motion is made. Additionally an examination of the rigid body LTI state matrices, Ref 33, supports this assumption of minimal cross coupling between the lateral (v_{B_x}, ω_{B_y}, and ω_{B_z}) and the longitudinal (v_{B_y}, v_{B_z}, and ω_{B_x}) states. An eigenvalue analysis of a representative HALE aircraft further supports this assumption.

The lateral and the longitudinal eigenvalues and eigenvectors of the B reference frame for a statically deformed aircraft at a given (heavy) fuel weight are presented in Tables 5 and 6. As it can be seen by examining the eigenvectors, there exists a fairly distinct separation of lateral and longitudinal motion. When the elastic states are included, a distinct change in the lateral eigenvalues and eigenvectors occurs, as seen in Table 7. The "Sideslip" and "Sideslip/Yaw Rate" modes experience a significant change in the eigenvalues and changes in the sign of the eigenvector components. However the real change is in the "Roll" mode as it no longer has any significant contribution from the rigid body roll rate, ω_{B_y}. But rather ω_{B_y} now contributes to various elastic strains and rates (not presented). Because of this, the elastic states are assumed to be tightly coupled with the rigid body lateral motion. The longitudinal eigenvalues and vectors also experience a change as seen in Table 8, with a major change in the "Vertical/Longitudinal" eigenvalue. This eigenvalue now has contributions of about 2% from several of the in and out of plane bending strain rates (not presented). However from Table 8, over 94.5% of the contribution comes from the B reference frame longitudinal states. Because of this significant contribution, it assumed that the longitudinal states are decoupled from the elastic states. While this strong coupling of lateral and elastic modes cannot be generalized for all very flexible aircraft, the analysis does hold for the representative aircraft used here at different loadings (fuel) conditions (not shown). In general, an eigenvalue and eigenvector analysis should be performed at nonlinear equilibrium conditions of a very flexible aircraft configuration to determine the coupling of elastic states with B reference frame motion. Based upon the outcome of the analysis, various linear and nonlinear control schemes could be utilized. For example, Gregory[22–25] has developed filtered nonlinear control techniques and optimum sensor placement for longitudinal control with coupled aeroelastic effects. In this dissertation a linear LQR formulation is developed for the lateral motion and a nonlinear dynamic inversion for the longitudinal motion.

2. *Lateral Motion Inner-Loop Controller*

Due to the inherent NMP zeros present in the lateral dynamics, Section III.A, most nonlinear control schemes are not sufficient for controlling it. Because of this, a traditional LQR controller is used for the inner-loop

Table 5. Lateral eigenvalues and eigenvectors for rigid body aircraft with elastically deformed wing

Name	Eigenvalue (rad/s)	Normalized Eigenvector	
Sideslip	$-2.5081 \cdot 10^{-4}$	$9.9729 \cdot 10^{-1}$	v_{B_x}
		$-4.0745 \cdot 10^{-12}$	v_{B_y}
		$5.4152 \cdot 10^{-13}$	v_{B_z}
		$2.9881 \cdot 10^{-14}$	ω_{B_x}
		$-2.3031 \cdot 10^{-3}$	ω_{B_y}
		$-7.3474 \cdot 10^{-2}$	ω_{B_z}
Sideslip/Yaw Rate	-1.0132	$9.9003 \cdot 10^{-1}$	v_{B_x}
		$1.9776 \cdot 10^{-15}$	v_{B_y}
		$5.4550 \cdot 10^{-15}$	v_{B_z}
		$1.8435 \cdot 10^{-14}$	ω_{B_x}
		$-5.8755 \cdot 10^{-2}$	ω_{B_y}
		$1.2801 \cdot 10^{-1}$	ω_{B_z}
Roll Rate	-6.7172	$2.9039 \cdot 10^{-2}$	v_{B_x}
		$-3.4145 \cdot 10^{-13}$	v_{B_y}
		$9.5019 \cdot 10^{-12}$	v_{B_z}
		$-8.7481 \cdot 10^{-13}$	ω_{B_x}
		$9.9957 \cdot 10^{-1}$	ω_{B_y}
		$4.8056 \cdot 10^{-3}$	ω_{B_z}

Table 6. Longitudinal eigenvalues and eigenvectors for rigid body aircraft with elastically deformed wing

Name	Eigenvalue (rad/s)	Normalized Eigenvector	
Vertical	-3.1402	$2.2795 \cdot 10^{-14}$	v_{B_x}
		$1.1025 \cdot 10^{-2}$	v_{B_y}
		$-9.9077 \cdot 10^{-1}$	v_{B_z}
		$1.3514 \cdot 10^{-1}$	ω_{B_x}
		$5.5100 \cdot 10^{-13}$	ω_{B_y}
		$6.9795 \cdot 10^{-15}$	ω_{B_z}
Vertical/Longitudinal	$-7.0227 \cdot 10^{-2}$	$5.3907 \cdot 10^{-13}$	v_{B_x}
		$-5.9205 \cdot 10^{-1}$	v_{B_y}
		$8.0334 \cdot 10^{-1}$	v_{B_z}
		$6.4225 \cdot 10^{-2}$	ω_{B_x}
		$-1.9984 \cdot 10^{-13}$	ω_{B_y}
		$-3.3784 \cdot 10^{-14}$	ω_{B_z}
Longitudinal	$1.8195 \cdot 10^{-2}$	$2.2961 \cdot 10^{-13}$	v_{B_x}
		$9.7330 \cdot 10^{-1}$	v_{B_y}
		$2.2882 \cdot 10^{-1}$	v_{B_z}
		$1.8057 \cdot 10^{-2}$	ω_{B_x}
		$2.3820 \cdot 10^{-14}$	ω_{B_y}
		$-1.7343 \cdot 10^{-14}$	ω_{B_z}

Table 7. Lateral eigenvalues and eigenvectors for flexible aircraft

Name	Eigenvalue (rad/s)	Normalized Eigenvector	
Sideslip	$-1.5489 \cdot 10^{-1}$	$-9.9566 \cdot 10^{-1}$	v_{B_x}
		$-6.4196 \cdot 10^{-13}$	v_{B_y}
		$-1.8588 \cdot 10^{-13}$	v_{B_z}
		$-2.3153 \cdot 10^{-14}$	ω_{B_x}
		$4.7108 \cdot 10^{-2}$	ω_{B_y}
		$-8.0219 \cdot 10^{-2}$	ω_{B_z}
Sideslip/Yaw Rate	$5.3050 \cdot 10^{-2}$	$-9.9163 \cdot 10^{-1}$	v_{B_x}
		$7.0617 \cdot 10^{-12}$	v_{B_y}
		$1.7969 \cdot 10^{-12}$	v_{B_z}
		$9.3405 \cdot 10^{-14}$	ω_{B_x}
		$-1.8629 \cdot 10^{-2}$	ω_{B_y}
		$1.2773 \cdot 10^{-1}$	ω_{B_z}

Table 8. Longitudinal eigenvalues and eigenvectors for flexible aircraft

Name	Eigenvalue (rad/s)	Normalized Eigenvector	
Vertical	-2.5686	$-1.2290 \cdot 10^{-12}$	v_{B_x}
		$2.0530 \cdot 10^{-1}$	v_{B_y}
		$-9.7172 \cdot 10^{-1}$	v_{B_z}
		$7.4426 \cdot 10^{-2}$	ω_{B_x}
		$-3.2549 \cdot 10^{-13}$	ω_{B_y}
		$-3.8281 \cdot 10^{-13}$	ω_{B_z}
Vertical/Longitudinal	-3.2479	$3.0616 \cdot 10^{-12}$	v_{B_x}
		$-2.5808 \cdot 10^{-1}$	v_{B_y}
		$9.0910 \cdot 10^{-1}$	v_{B_z}
		$2.3189 \cdot 10^{-2}$	ω_{B_x}
		$1.2535 \cdot 10^{-12}$	ω_{B_y}
		$9.3817 \cdot 10^{-13}$	ω_{B_z}
Longitudinal	$4.7465 \cdot 10^{-2}$	$-5.5698 \cdot 10^{-12}$	v_{B_x}
		$-9.7008 \cdot 10^{-1}$	v_{B_y}
		$-2.4244 \cdot 10^{-1}$	v_{B_z}
		$-1.2841 \cdot 10^{-2}$	ω_{B_x}
		$-8.6632 \cdot 10^{-14}$	ω_{B_y}
		$6.6309 \cdot 10^{-13}$	ω_{B_z}

lateral motion. For the lateral controller, full state feedback was assumed, where the states to be controlled are

$$x_{lat} = \begin{bmatrix} \epsilon^T & \dot{\epsilon}^T & v_{B_x} & \omega_{B_y} & \omega_{B_z} \end{bmatrix}^T \tag{63}$$

While the assumption of full elastic state feedback (ϵ and $\dot{\epsilon}$) may present a practical limitation, it is used here as a starting point for very flexible aircraft control architecture development. Linear time invariant A and B matrices are generated from Eq. 14 for the lateral states of Eq. 63. Error states are then augmented to the system such that

$$x_{lat} = \begin{bmatrix} \epsilon^T & \dot{\epsilon}^T & v_{B_x} & \omega_{B_y} & \omega_{B_z} & e_{lat}^T \end{bmatrix}^T \tag{64}$$

and

$$\dot{e}_{lat} = \begin{Bmatrix} v_{B_x} - 0 \\ \omega_{B_y} - \omega_{B_y com} \\ \omega_{B_z} - \omega_{B_z com} \end{Bmatrix} \tag{65}$$

The augmented system can then be represented as

$$\dot{x}_{lat} = \begin{bmatrix} A_{lat} & 0 \\ C_{lat} & 0 \end{bmatrix} x_{lat} + \begin{bmatrix} B_{lat} \\ 0 \end{bmatrix} u_{lat} + \begin{bmatrix} 0 \\ -I \end{bmatrix} \begin{Bmatrix} 0 \\ \omega_{B_y com} \\ \omega_{B_z com} \end{Bmatrix} \tag{66}$$

where

$$C_{lat} = \begin{bmatrix} 0 & 0 & 1 & 0 & 0 \\ 0 & 0 & 0 & 1 & 0 \\ 0 & 0 & 0 & 0 & 1 \end{bmatrix} \tag{67}$$

The lateral control vector is found using the control law

$$u_{lat} = -\begin{bmatrix} K_{lat} & K_{e_{lat}} \end{bmatrix} \begin{Bmatrix} x_{lat} \\ e_{lat} \end{Bmatrix} \tag{68}$$

where K_{lat} and $K_{e_{lat}}$ are found using standard LQR techniques applied to the augmented system of Eq. 66.

3. Longitudinal Motion Inner-Loop Controller

In a similar manner to Al-Hiddabi[49] and Al-Hiddabi and McClamroch,[50] partial feedback linearization or dynamic inversion is used for development of the very flexible aircraft. Here dynamic inversion is applied to the longitudinal states of interest, i.e.,

$$x_{long} = \begin{bmatrix} v_{B_y} & v_{B_z} & \omega_{B_x} \end{bmatrix}^T \tag{69}$$

Dynamic inversion[51,52] is a process by which nonlinear differential equations of the form

$$\begin{aligned} \dot{x} &= f(x) + g(x)u \\ y &= h(x) \end{aligned} \tag{70}$$

are transformed into an equivalent linear form

$$\dot{\chi} = v \tag{71}$$

The transformation is accomplished by first making a change of variables

$$\chi = y \tag{72}$$

and then finding $\dot{\chi}$

$$\begin{aligned} \dot{\chi} = \dot{y} &= \frac{\partial h}{\partial x}\dot{x} \\ &= \frac{\partial h}{\partial x} f(x) + \frac{\partial h}{\partial x} g(x)u \end{aligned} \tag{73}$$

A new control variable, v, is then defined as

$$v = \frac{\partial h}{\partial x} f(x) + \frac{\partial h}{\partial x} g(x) u \tag{74}$$

and finally solving for u

$$u = \left[\frac{\partial h}{\partial x} g(x) \right]^{-1} \left(v - \frac{\partial h}{\partial x} f(x) \right) \tag{75}$$

The transformed system, Eq. 71, can then be augmented with error states if desired, and the control variable, v is solved as

$$v = -K\chi \tag{76}$$

using any number of linear controller techniques, yielding closed loop trajectory tracking.

For the very flexible aircraft, a subset of the linear and angular body velocities, β, are desired to be controlled, Eq. 69, using dynamic inversion. To accomplish this, β is found from the EOM for ϵ and β. Starting with Eq. 14,

$$\begin{bmatrix} M_{FF} & M_{FB} \\ M_{BF} & M_{BB} \end{bmatrix} \begin{Bmatrix} \ddot{\epsilon} \\ \dot{\beta} \end{Bmatrix} = -\begin{bmatrix} C_{FF} & C_{FB} \\ C_{BF} & C_{BB} \end{bmatrix} \begin{Bmatrix} \dot{\epsilon} \\ \beta \end{Bmatrix} - \begin{Bmatrix} K_{FF}\epsilon \\ 0 \end{Bmatrix} + \begin{Bmatrix} R_F \\ R_B \end{Bmatrix} \tag{77}$$

these can be solved by inverting the generalized mass matrix. Using Fact 2.15.3 of Ref. 53

$$\begin{bmatrix} A & B \\ B^T & C \end{bmatrix}^{-1} = \begin{bmatrix} \left(A - BC^{-1}B^T\right)^{-1} & -\left(A - BC^{-1}B^T\right)^{-1} BC^{-1} \\ -C^{-1}B^T \left(A - BC^{-1}B^T\right)^{-1} & C^{-1}B^T \left(A - BC^{-1}B^T\right)^{-1} BC^{-1} + C^{-1} \end{bmatrix} \tag{78}$$

and noting $M_{FB} = M_{BF}^T$ from Eq. 7, the inverse of the generalized mass matrix of Eq. 77 is

$$\begin{bmatrix} M_{FF} & M_{FB} \\ M_{BF} & M_{BB} \end{bmatrix}^{-1} = \begin{bmatrix} Q_M & -Q_M M_{FB} M_{BB}^{-1} \\ -M_{BB}^{-1} M_{BF} Q_M & M_{BB}^{-1} M_{BF} Q_M M_{FB} M_{BB}^{-1} + M_{BB}^{-1} \end{bmatrix} \tag{79}$$

where

$$Q_M = \left(M_{FF} - M_{FB} M_{BB}^{-1} M_{BF}\right)^{-1} \tag{80}$$

Therefore $\ddot{\epsilon}$ and $\dot{\beta}$ are given by

$$\ddot{\epsilon} = -C_{11}\dot{\epsilon} - C_{12}\beta - Q_M K_{FF}\epsilon + R_{F1} \tag{81}$$

$$\dot{\beta} = -C_{22}\beta - C_{21}\dot{\epsilon} + R_{B1} \tag{82}$$

where

$$\begin{aligned} C_{11} &= Q_M C_{FF} - Q_M M_{FB} M_{BB}^{-1} C_{BF} \\ C_{12} &= Q_M C_{FB} - Q_M M_{FB} M_{BB}^{-1} C_{BB} \\ C_{21} &= -M_{BB}^{-1} M_{BF} Q_M C_{FF} + \left(M_{BB}^{-1} M_{BF} Q_M M_{FB} M_{BB}^{-1} + M_{BB}^{-1}\right) C_{BF} \\ C_{22} &= -M_{BB}^{-1} M_{BF} Q_M C_{FB} + \left(M_{BB}^{-1} M_{BF} Q_M M_{FB} M_{BB}^{-1} + M_{BB}^{-1}\right) C_{BB} \\ R_{F1} &= Q_M R_F - Q_M M_{FB} M_{BB}^{-1} R_B \\ R_{B1} &= -M_{BB}^{-1} M_{BF} Q_M R_F + \left(M_{BB}^{-1} M_{BF} Q_M M_{FB} M_{BB}^{-1} + M_{BB}^{-1}\right) R_B \end{aligned} \tag{83}$$

The generalized force vectors, R_F and R_B, can be further expanded into a control affine form

$$R_F = R_{F_{u=0}}(\epsilon, \dot{\epsilon}, \beta, \zeta, \lambda) + R_{F_u}(\epsilon, \dot{\epsilon}, \beta, \zeta, \lambda) u \tag{84}$$

$$R_B = R_{B_{u=0}}(\epsilon, \dot{\epsilon}, \beta, \zeta, \lambda) + R_{B_u}(\epsilon, \dot{\epsilon}, \beta, \zeta, \lambda) u \tag{85}$$

The body velocity, Eq. 82, can then be written in the generalized form

$$\dot{\beta} = f_\beta + g_\beta u \tag{86}$$

where

$$\begin{aligned} f_\beta &= -C_{22}\beta - C_{21}\dot{\epsilon} + -M_{BB}^{-1}M_{BF}Q_M R_{F_{u=0}} + \\ &\quad + \left(M_{BB}^{-1}M_{BF}Q_M M_{FB}M_{BB}^{-1} + M_{BB}^{-1}\right) R_{B_{u=0}} \end{aligned} \tag{87}$$

and

$$g_\beta = -M_{BB}^{-1}M_{BF}Q_M R_{F_u} + \left(M_{BB}^{-1}M_{BF}Q_M M_{FB}M_{BB}^{-1} + M_{BB}^{-1}\right) R_{B_u} \tag{88}$$

Stability of dynamic inversion requires the so-called internal or zero dynamics[54] to be stable. For the partial Dynamic Inversion scheme proposed, the internal dynamics consist of the controlled lateral states and the uncontrolled inflow states.[32] The assumption is made that the internal dynamic states are stable. This assumption is valid provided the linear controller of Section III.D.2 yields closed loop stability and the inflow states, λ, are not driven unstable due to the aeroelastic boundaries of flutter and divergence. While avoiding the aeroelastic boundaries is a limitation of the current design, it is a necessary requirement in the developing stages of controller design for very flexible aircraft.

The longitudinal outputs to be tracked, Eq. 69, can be written as

$$y_{long} = C_{long}\beta \tag{89}$$

where

$$C_{long} = \begin{bmatrix} 0 & 1 & 0 & 0 & 0 & 0 \\ 0 & 0 & 1 & 0 & 0 & 0 \\ 0 & 0 & 0 & 1 & 0 & 0 \end{bmatrix} \tag{90}$$

The linearized form is

$$\dot{\chi}_{long} = v_{long} \tag{91}$$

where

$$u_{long} = g_\beta^{-1}\left(v_{long} - f_\beta\right) \tag{92}$$

The system is then augmented with longitudinal error states

$$\dot{e}_{long} = \begin{Bmatrix} v_{B_y} - v_{B_y com} \\ v_{B_z} - v_{B_z com} \\ \omega_{B_x} - \omega_{B_x com} \end{Bmatrix} \tag{93}$$

and the final linearized system is

$$\begin{Bmatrix} \dot{\chi}_{long} \\ \dot{e}_{long} \end{Bmatrix} = \begin{bmatrix} 0 & 0 \\ C_{long} & 0 \end{bmatrix} \begin{Bmatrix} \chi_{long} \\ e_{long} \end{Bmatrix} + \begin{bmatrix} I \\ 0 \end{bmatrix} \{v_{long}\} + \begin{bmatrix} 0 \\ -I \end{bmatrix} \begin{Bmatrix} v_{B_y com} \\ v_{B_z com} \\ \omega_{B_x com} \end{Bmatrix} \tag{94}$$

The control variable, v_{long}, is then computed using full state feedback as

$$v_{long} = -\begin{bmatrix} K_{\chi_{long}} & K_{e_{long}} \end{bmatrix} \begin{Bmatrix} \chi_{long} \\ e_{long} \end{Bmatrix} \tag{95}$$

where the gains, $K_{\chi_{long}}$ and $K_{e_{long}}$, are computed using the LQR technique. The actual control signal, u_{long} is computed using Eq. 92.

Finally, since dynamic inversion becomes unstable with the introduction of NMP zeros,[55] flight path angle is tracked, instead of altitude, in the outer-loop design to prevent the introduction of NMP zeros into the inner-loop longitudinal dynamics. This is necessary since in traditional wing/body/tail aircraft an increase in altitude is accomplished by deflecting the trailing edge surface of the elevator upwards. This creates a downward force which temporarily decreases the overall aircraft lift and a subsequent decrease in altitude. However, this downward force also creates a nose up pitching moment, which increases the angle of attack.

Once the airflow adjusts to this increase in angle of attack, overall lift is increased and the aircraft begins to climb. In mathematical terms, this behavior represents a NMP system. To control altitude a first-order approximation of the rate of climb, $\dot{h}$, is used

$$\dot{h} = V\gamma \tag{96}$$

By prescribing the altitude and total velocity, V, trajectories, $\dot{h}$, γ, and $\dot{\gamma}$ can be commanded to the outer-loop.

IV. Trajectory Control Studies

In this section, trajectory control studies are performed on the proposed controller architecture. The control architecture is initially applied to an elastic aircraft at a heavy weight condition. Simulated climbs, bank angle changes, and climb and turning trajectories are presented and discussed. The controller is then applied, without changes to any of the gains, to a light weight condition which has a commanded climb and turn trajectory. Finally a representative mission profile segment is developed and simulated.

A. Representative HALE Aircraft

For the aircraft simulation studies, a representative HALE type aircraft was created and it is shown in Figure 5. The relevant physical properties are summarized in Table 9. The vehicle was designed to be

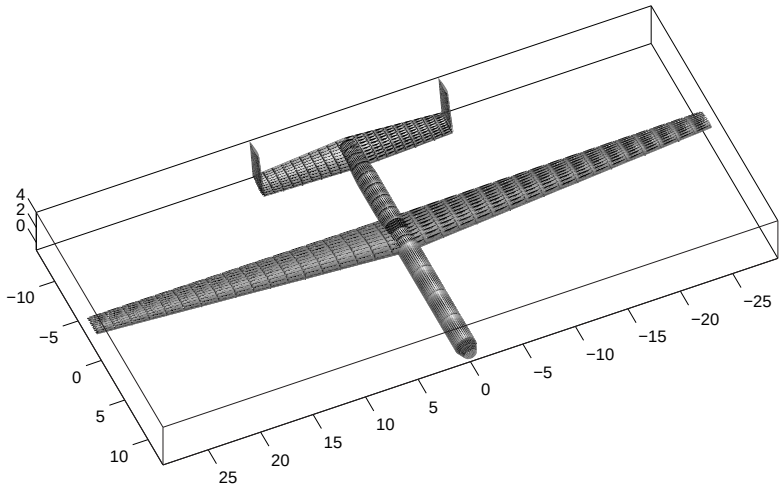

Figure 5. Representative HALE aircraft model (units are in meters)

statically stable for moderate wing deflections in both the longitudinal and lateral axes. Table 10 also includes the trimmed longitudinal controls and state (elevator angle, thrust level, angle of attack) for both a gliding and 1-g level flights. Additional details of the vehicle's mass, structural damping, and stiffness parameters are provided in Ref. 33.

The vehicle is a conventional wing/body/tail configuration with twin vertical tails. It is representative of a HALE aircraft concept being considered by the USAF. The aircraft has the conventional control surfaces of elevator, aileron, and twin rudders. The elevator is such that a positive elevator control input, δ_e, results in a negative pitching moment (nose down). The left and right ailerons have a -1:1 gearing ratio, such that a positive aileron control input, δ_a, results in a roll to the left (left wing down). The twin rudders have a 1:1 gear ratio such that a positive rudder control input, δ_r, produces a positive yawing moment (nose left). Recall the B reference frame orientation is x positive out the right wing, y positive out the nose, and z positive up. Thrust is accomplished using a simple point force applied at the origin of the B reference

Table 9. Geometric properties of the very flexible aircraft model

Model Parameters		
Property	Value	Units
Fuselage Length	26.4	m
Wing Span	58.6	m
Wing Area	196.3	m^2
Root Chord	4.5	m
Tip Chord	2.2	m
Aspect Ratio	17.5	—
Wing Incidence Angle	3.0°	—
Horizontal Tail Span	18.0	m
Horizontal Root Chord	3.5	m
Horizontal Tip Chord	2.45	m
Horizontal Tail Incidence Angle	−4.5°	—
Vertical Tail Span	4.0	m
Vertical Root Chord	2.45	m
Vertical Tip Chord	2.0	m
Wing/Horizontal Tail Airfoil	NACA 4415	—
Vertical Tail Airfoil	NACA 0012	—
Aileron Location	16.3 to 22.8	m
Aileron, Elevator, Rudder Chord	$0.2c_{local}$	
Elevator Span Location	1.8 to 9.0	m
Rudder Span Location	0.8 to 3.2	m
Elements per wing	9	—
Elements per horizontal tail	5	—
Elements per vertical tail	5	—
Elements in fuselage	10	—
Total Number of Elements	48	—
Number of second-order states	192	—
Number of first-order states	241	—

Table 10. Control and aircraft states and inertia properties of the very flexible aircraft model

Model Parameters					
Property	Value				Units
	Light, no thrust	Heavy, no thrust	Light, thrust for level flight	Heavy, thrust for level flight	
Elevator deflec. angle, δ_e	$4.51°$	$-16.80°$	$-6.89°$	$-13.68°$	—
Thrust rqd., δ_t	0	0	$3.21 \cdot 10^4$	$1.12 \cdot 10^5$	N
Aircraft angle of attack, α	$0.80°$	$7.62°$	$1.93°$	$7.30°$	—
Fuel mass	0	$32,000$	0	$32,000$	kg
Total mass	$2.10 \cdot 10^4$	$5.38 \cdot 10^4$	$2.10 \cdot 10^4$	$5.38 \cdot 10^4$	kg
Fuel fraction	0.0	59.5	0.0	59.5	%
I^{ss}_{xx} *	$1.48 \cdot 10^6$	$1.75 \cdot 10^6$	$1.49 \cdot 10^6$	$1.75 \cdot 10^6$	$\text{kg} \cdot \text{m}^2$
I^{ss}_{yy}	$8.20 \cdot 10^5$	$2.93 \cdot 10^6$	$8.19 \cdot 10^5$	$2.93 \cdot 10^6$	$\text{kg} \cdot \text{m}^2$
I^{ss}_{zz}	$2.27 \cdot 10^6$	$4.46 \cdot 10^6$	$2.26 \cdot 10^6$	$4.47 \cdot 10^6$	$\text{kg} \cdot \text{m}^2$
I^{ss}_{xy}	0	0	0	0	$\text{kg} \cdot \text{m}^2$
I^{ss}_{xz}	0	0	0	0	$\text{kg} \cdot \text{m}^2$
I^{ss}_{yz}	$1.82 \cdot 10^4$	$9.20 \cdot 10^4$	$2.06 \cdot 10^4$	$9.00 \cdot 10^4$	$\text{kg} \cdot \text{m}^2$
x_{cm}	0	0	0	0	m
y_{cm}	3.13	$4.33 \cdot 10^{-3}$	3.14	$5.64 \cdot 10^{-3}$	m
z_{cm}	0.29	0.79	0.34	0.77	m

*Note: I^{ss} are the inertia properties in a deformed steady state configuration
Note: All aircraft simulations are begun at sea level conditions and $65 m/s$ level flight

frame and in the y direction, such that a positive thrust input, δ_t results in an acceleration in the positive y direction.

B. Representative Flexible Aircraft Trajectory Tracking

Flexible aircraft trajectory tracking studies are presented here. A single controller is presented and applied to trajectory control for climb only, bank only, and simultaneous climb and bank all at a given (heavy) fuel state. The controller is then applied at an alternate (empty) fuel state demonstrating its robustness to significant mass and inertia changes. Finally a representative mission profile is simulated.

1. *Flexible Aircraft Controller Design*

The two separate inner-loop controllers for a flexible aircraft were presented in Section III.D.1. For the longitudinal motion, a dynamic inversion approach was developed. There the longitudinal states used in development of the controller were longitudinal and vertical velocity (v_{B_y} and v_{B_z}) and pitch rate, ω_{B_x}. The corresponding control inputs were elevator, δ_e, and throttle, δ_t. Initially all three longitudinal states were attempted to be controlled through the use of a pseudo-inverse of the resulting control effector matrix function, $\left[\frac{\partial h}{\partial x} g(x)\right]$, Eq. 75. The use of the pseudo inverse resulted in a stable inner-loop longitudinal controller, but it had poor tracking performance. A significant improvement is achieved by only controlling v_{B_y} and ω_{B_x}. The resulting set of error states are modified from the proposed set, Eq. 93 to

$$\dot{e}_{long} = \left\{ \begin{array}{c} v_{B_y} - v_{B_y com} \\ \omega_{B_x} - \omega_{B_x com} \end{array} \right\}. \tag{97}$$

The resulting inner-loop longitudinal state vector is

$$\chi_{long} = \left\{ \begin{array}{c} v_{B_y} \\ \omega_{B_x} \\ e_{long} \end{array} \right\}. \tag{98}$$

A standard LQR controller is applied to the resulting LTI state space system (see Section 3 for details) where the weighting matrices are

$$Q_{long} = \text{diag}\left[\begin{array}{cccc} 1 & 1 & 10^2 & 10^4 \end{array} \right] \tag{99}$$

$$R_{long} = \text{diag}\left[\begin{array}{cc} 1 & 1 \end{array} \right]. \tag{100}$$

For the lateral inner-loop controller, the error states are also modified from Eq. 101 to

$$\dot{e}_{lat} = \left\{ \begin{array}{c} v_{B_x} - 0 \\ \omega_{B_y} - \omega_{B_y com} \end{array} \right\}. \tag{101}$$

This was done for two reasons. First, due to the addition of the strain, ϵ, and strain rate, $\dot{\epsilon}$, states to the lateral inner-loop state vector, Eq. 64, it is difficult to find weighting matrices Q and R which provide solutions to the ARE of the LQR technique. Removal of the yaw rate state assisted this problem. Second, it was found that commanding the states of lateral velocity, v_{B_x}, and roll rate, ω_{B_y}, provided stable tracking of the removed yaw rate, ω_{B_z}. As described in Section III.D.2, a LQR controller is applied to the lateral motion inner-loop states. The weighting matrices are

$$Q_{lat} = \text{diag}\left[\begin{array}{ccccc} Q_\epsilon & Q_{v_{B_x}} & Q_{\omega_{B_y}} & Q_{\omega_{B_z}} & Q_{e_{lat}} \end{array} \right] \tag{102}$$

$$R_{lat} = \text{diag}\left[\begin{array}{cc} 1 & 1 \end{array} \right] \tag{103}$$

where

$$\begin{aligned} Q_{\epsilon} &= 10^{-3}, \\ Q_{v_{B_x}} &= 0, \\ Q_{\omega_{B_y}} &= 10, \\ Q_{\omega_{B_z}} &= 0, \\ Q_{e_{lat}} &= \begin{bmatrix} 10^2 & 10^3 \end{bmatrix}. \end{aligned} \tag{104}$$

The outer-loop gains, described in Section III.D.3, are loosely designed using the guidelines of Ziegler and Nichols.[44,45] The final chosen values are

$$k_{\Phi} = 0.9; \quad k_{I\Phi} = 0.225; \quad k_{d\Phi} = 0.45, \tag{105}$$

$$k_{\dot{\Phi}} = 0.9; \quad k_{I\dot{\Phi}} = 0.225; \quad k_{II\dot{\Phi}} = 0.0225, \tag{106}$$

$$k_{\gamma} = 0.5; \quad k_{I\gamma} = 0.5; \quad k_{II\gamma} = 0, \quad k_{d\gamma} = 0.05; \tag{107}$$

$$k_{\dot{\gamma}} = 0.5; \quad k_{I\dot{\gamma}} = 0.5; \quad k_{II\dot{\gamma}} = 0.1. \tag{108}$$

Finally due to high-frequency numerical error occurring during the first few time steps of the simulations, a third-order low-pass butterworth filter[56] was applied to the difference equations of flight path angle, γ, and Euler bank angle, Φ, and their rates given in Eq. 60. The filtered equation for the commanded flight path elevation angle difference is

$$\begin{aligned} \dot{x}_{\gamma_{com}} &= A_f x_{\gamma_{com}} + B_f \gamma_{com} \\ (\gamma_{com})_f &= C_f x_{\gamma_{com}}. \end{aligned} \tag{109}$$

For the third-order 2-Hz low-pass butterworth filter used, the state space matrices are

$$\begin{aligned} A_f &= \begin{bmatrix} -\pi & 0 & 0 \\ \pi & -\pi & -\pi \\ 0 & \pi & 0 \end{bmatrix}, \\ B_f &= \begin{Bmatrix} \pi \\ 0 \\ 0 \end{Bmatrix}, \\ C_f &= \begin{bmatrix} 0 & 0 & 1 \end{bmatrix}. \end{aligned} \tag{110}$$

The resulting outer-loop flight path and Euler bank angle commands are modified from Eq. 61 to

$$\begin{aligned} \Delta\gamma_{com} &= k_{\gamma}(\Delta\gamma)_f + k_{I\gamma}\int_0^t (\Delta\gamma)\,d\tau + k_{II\gamma}\int_0^t \left(\int_0^t (\Delta\gamma)\,d\tau\right) d\tau + k_{d\gamma}(\Delta\dot{\gamma})_f, \\ \Delta\dot{\gamma}_{com} &= k_{\dot{\gamma}}(\Delta\dot{\gamma})_f + k_{I\dot{\gamma}}(\Delta\gamma)_f + k_{II\dot{\gamma}}\int_0^t (\Delta\gamma)\,d\tau + k_{III\dot{\gamma}}\int_0^t \left(\int_0^t (\Delta\gamma)\,d\tau\right) d\tau, \\ \Delta\Phi_{com} &= k_{\Phi}(\Delta\Phi)_f + k_{I\Phi}\int_0^t (\Delta\Phi)\,d\tau + k_{d\Phi}\Delta\dot{\Phi}_f, \\ \Delta\dot{\Phi}_{com} &= k_{\dot{\Phi}}(\Delta\dot{\Phi})_f + k_{I\dot{\Phi}}(\Delta\Phi)_f + k_{II\dot{\Phi}}\int_0^t (\Delta\Phi)\,d\tau. \end{aligned} \tag{111}$$

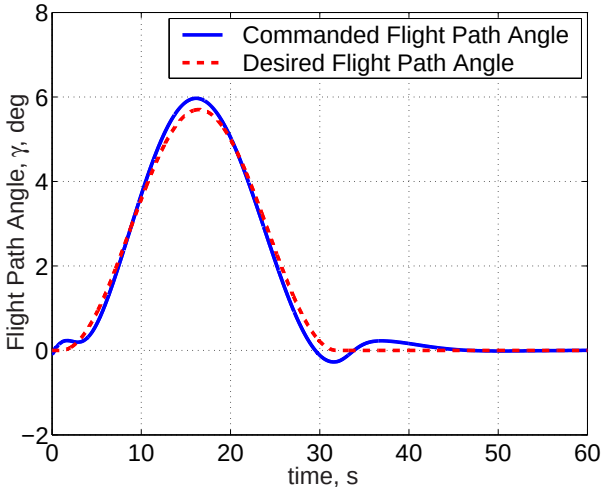

(a) Flight path angle

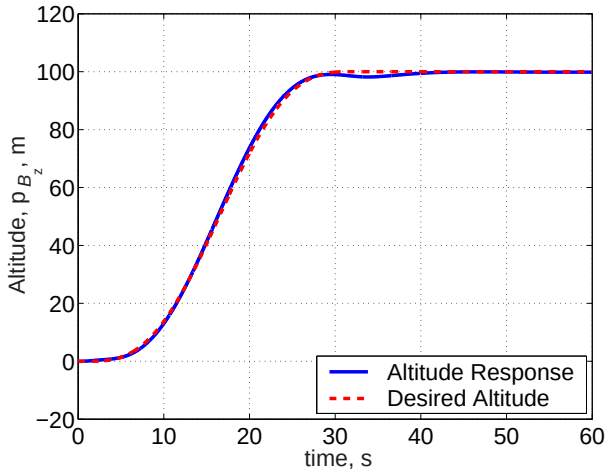

(b) Altitude

Figure 6. Commanded flight path angle and altitude, heavy weight condition, climb command

2. *Climb Only*

Here the flexible aircraft is commanded to make a 100 m climb in 31 s following a modified cosine input. Figure 6 shows that both the altitude and flight path angle have excellent tracking to the commands. The steady altitude error is less than 0.5 m. The longitudinal control inputs are shown in Figure 7. Other than high-frequency oscillations due to numerical initialization error seen in the elevator command, Figure 7a, the longitudinal control inputs are reasonable and reach steady state values upon completion of the climb. The longitudinal states are shown in Figure 8 and 9 along with the desired and commanded values. Here

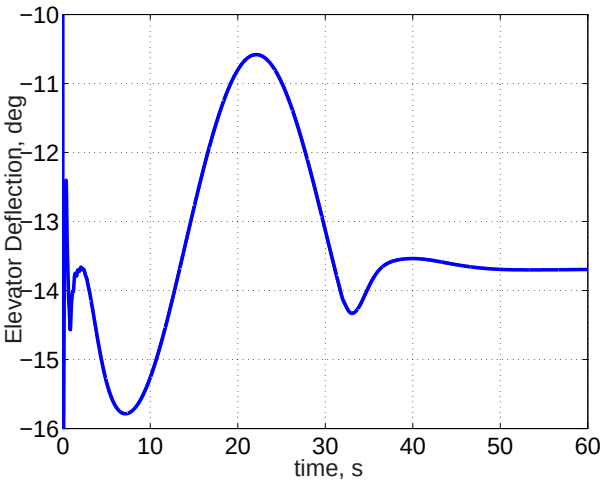

(a) Elevator

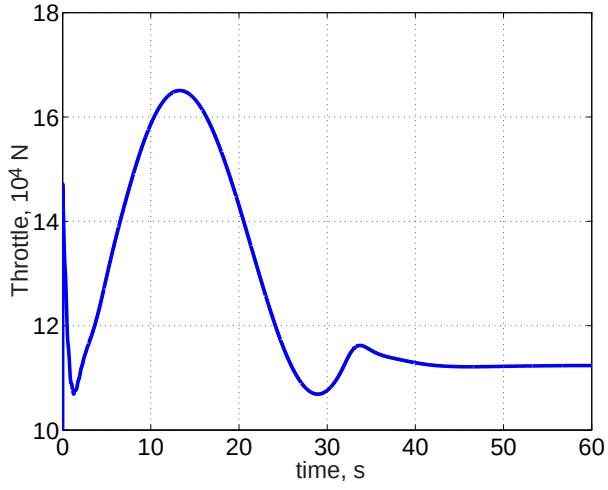

(b) Throttle

Figure 7. Longitudinal flight controls, heavy weight condition, climb command

excellent tracking is seen for the longitudinal velocity, v_{B_y}. For the vertical velocity there is no commanded value, only a desired trajectory derived from the desired altitude trajectory, Figure 6b, and the nonlinear transformations described in Section III.D.3. The closed loop controller provides a stable vertical velocity, as seen by its asymptotic convergence to the desired steady state value. Finally the aircraft response, inner loop command, and desired pitch rate, ω_{B_x}, are shown in Figure 9. The effect of the low-pass butterworth filter is seen by examining the commanded pitch rate and the simulated pitch rate response. Overall the use of the dynamic inversion on the longitudinal inner-loop dynamics is shown to work very well. Additionally

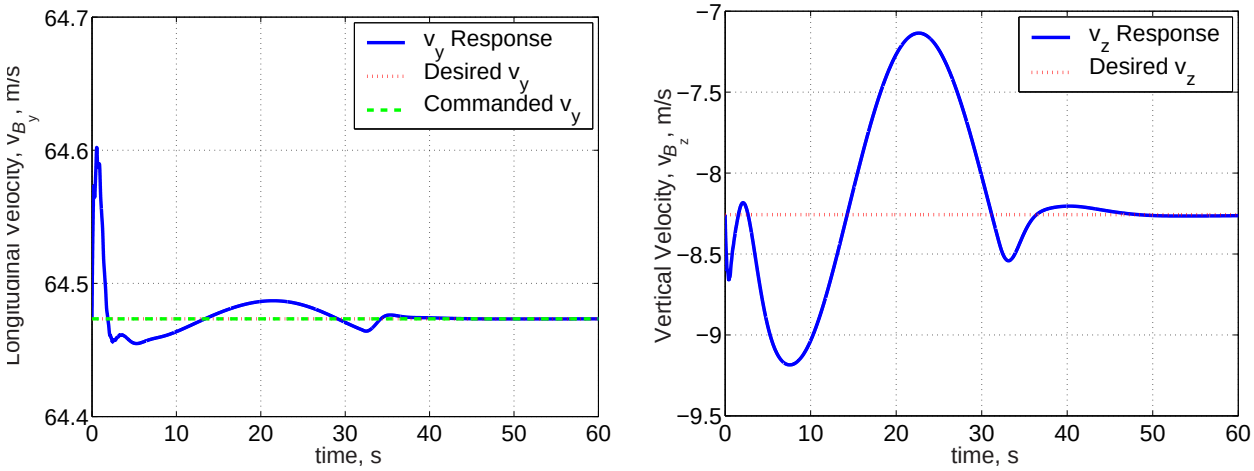

(a) Longitudinal velocity

(b) Vertical velocity

Figure 8. *B* **reference frame velocities, heavy weight condition, climb command**

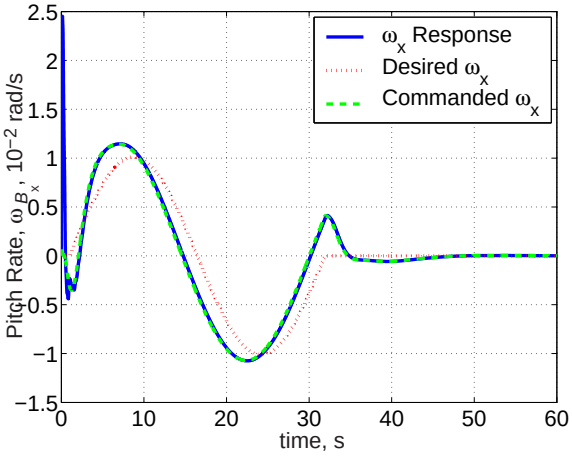

Figure 9. *B* **reference pitch rate actual, desired, and commanded for heavy weight, climb command**

this example shows that the assumption that longitudinal dynamics may be decoupled from the elastic states was valid for the representative aircraft.

3. *Bank Only*

Next a commanded change in Euler bank angle of 20° while maintaining level flight is simulated. The desired trajectories and aircraft response of flight path angle, altitude, and bank angle are seen in Figure 10. It is immediately apparent that the longitudinal and lateral coupling is excited by the subsequent change in flight path angle and altitude. However, despite an almost 25 m change in altitude, the altitude is controlled via the flight path angle. Additionally this change in altitude is within commercial pilot procedures, and subsequently would not create a problem if the aircraft were flying in the National Airspace system. The corresponding

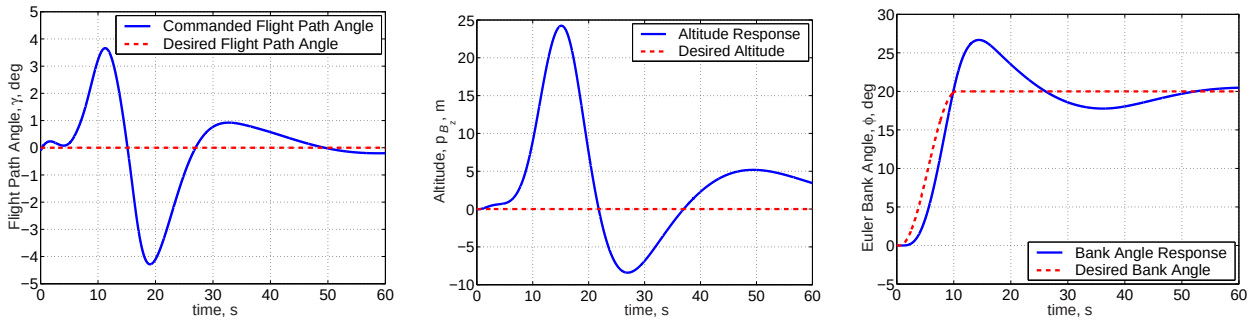

(a) Flight Path Angle (b) Altitude (c) Euler Bank Angle

Figure 10. Commanded flight path angle, altitude, and Euler angle for heavy weight condition, bank command

longitudinal and lateral control inputs are shown in Figures 11 and 12. Steady state changes are seen in the

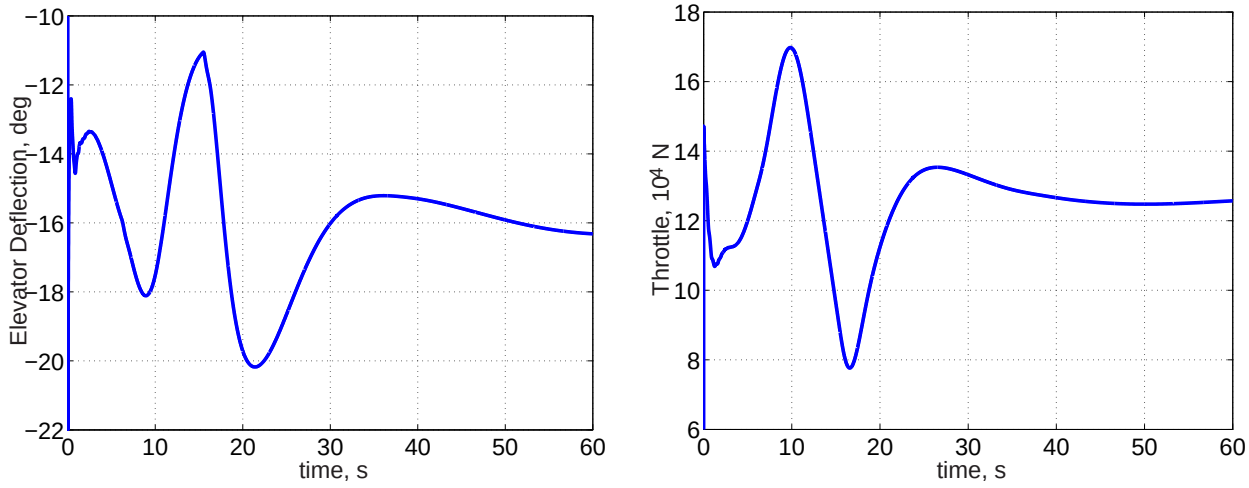

(a) Elevator (b) Throttle

Figure 11. Longitudinal flight controls, heavy weight condition, bank command

elevator and throttle from an initial wings level values of $-13.68°$ and $1.12 \cdot 10^5 N$, Table 9, to approximately $-16.5°$ and $1.25 \cdot 10^5 N$. Figure 12 shows that the lateral control inputs tend to steady state values required to maintain a level turn configuration. The controller also performed well in smoothly controlling the lateral motion states and the longitudinal velocity as seen in Figures 13, 14, and 15. The dynamic inversion inner-loop controller again shows excellent tracking between commanded and simulated response, Figure 13b and 15a. The oscillations of the longitudinal motion about desired trajectories (Figures 13a, b, and 15a) are attributed to the difficulty in tuning the nonlinear outer-loop controller when a lateral motion (bank angle here) is commanded. However despite this difficulty, the controller does exhibit stable tracking.

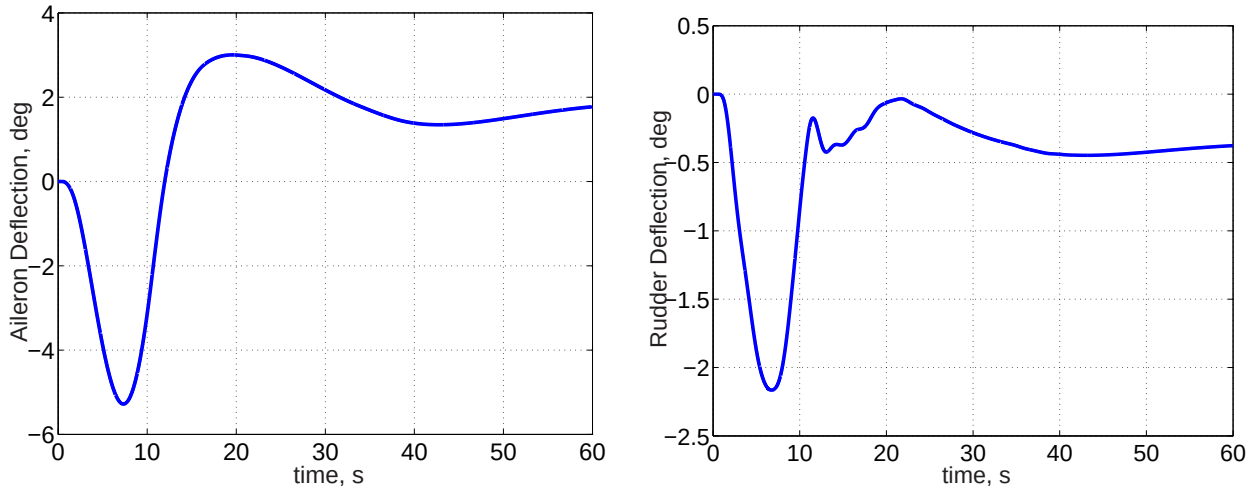

(a) Aileron (b) Rudder

Figure 12. Lateral flight controls, heavy weight condition, bank command

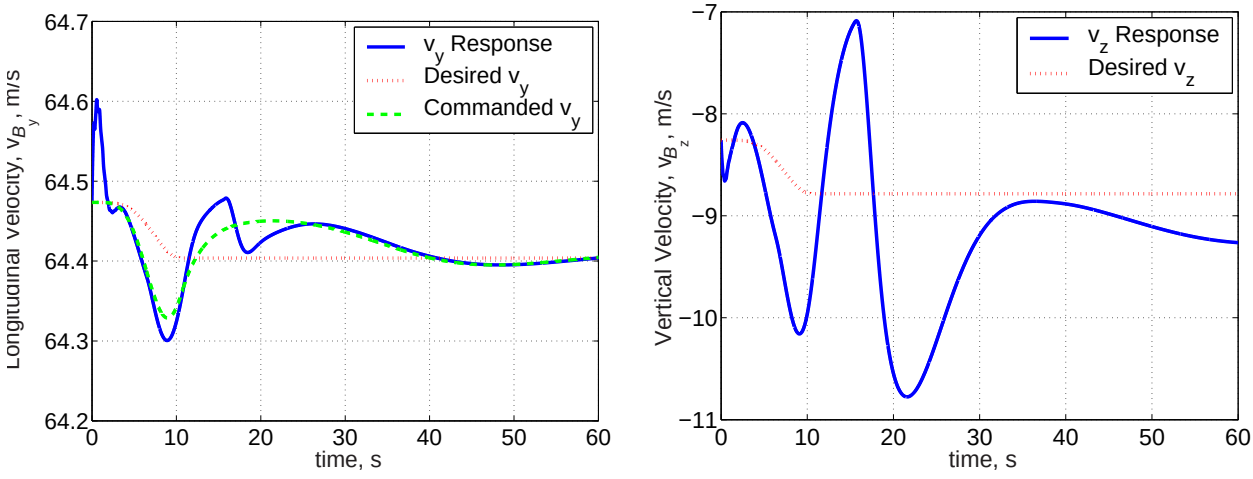

(a) Longitudinal velocity (b) Vertical velocity

Figure 13. B reference frame velocities, heavy weight condition, bank command

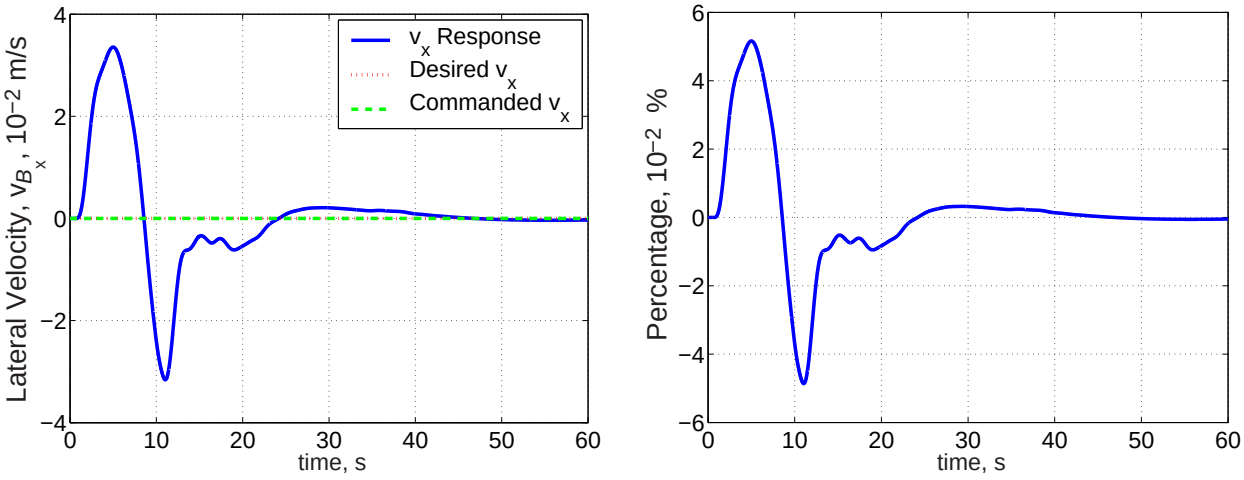

(a) Lateral velocity (b) Lateral velocity as a percentage of total velocity

Figure 14. *B* **reference frame lateral velocity, heavy weight condition, bank command**

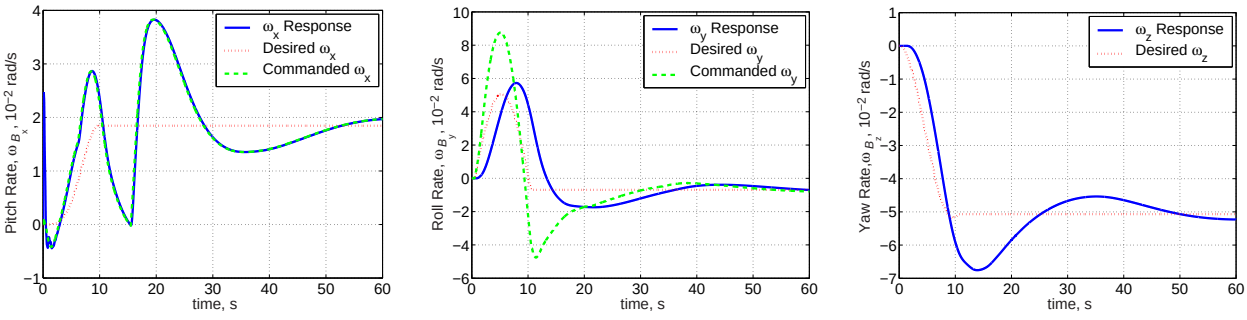

(a) Pitch Rate (b) Roll Rate (c) Yaw Rate

Figure 15. *B* **reference frame angular velocities, heavy weight condition, bank command**

4. Bank and Climb

Finally for the heavy weight fuel condition, a combined climb and turn trajectory is commanded. The flight path angle, altitude, and bank angle change trajectories are seen in Figure 16. The corresponding

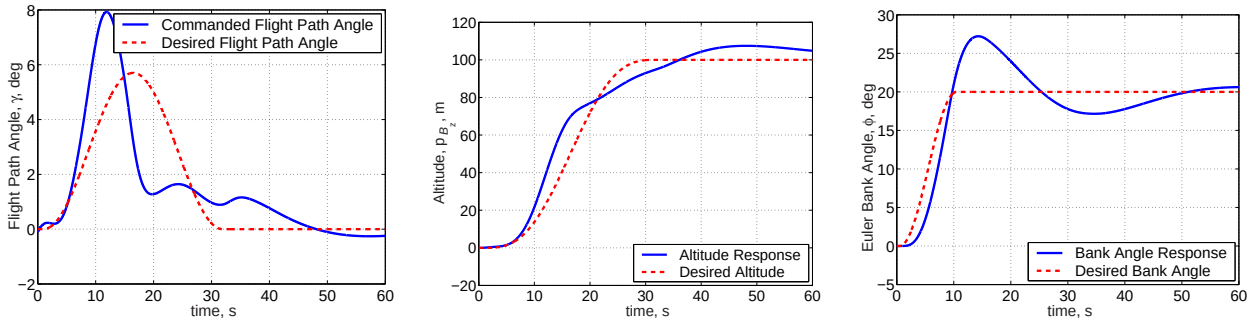

(a) Flight Path Angle (b) Altitude (c) Euler Bank Angle

Figure 16. Commanded flight path angle, altitude, and Euler angle for heavy weight condition, bank/climb command

longitudinal and lateral control inputs are shown in Figures 17 and 18. The B reference frame linear and

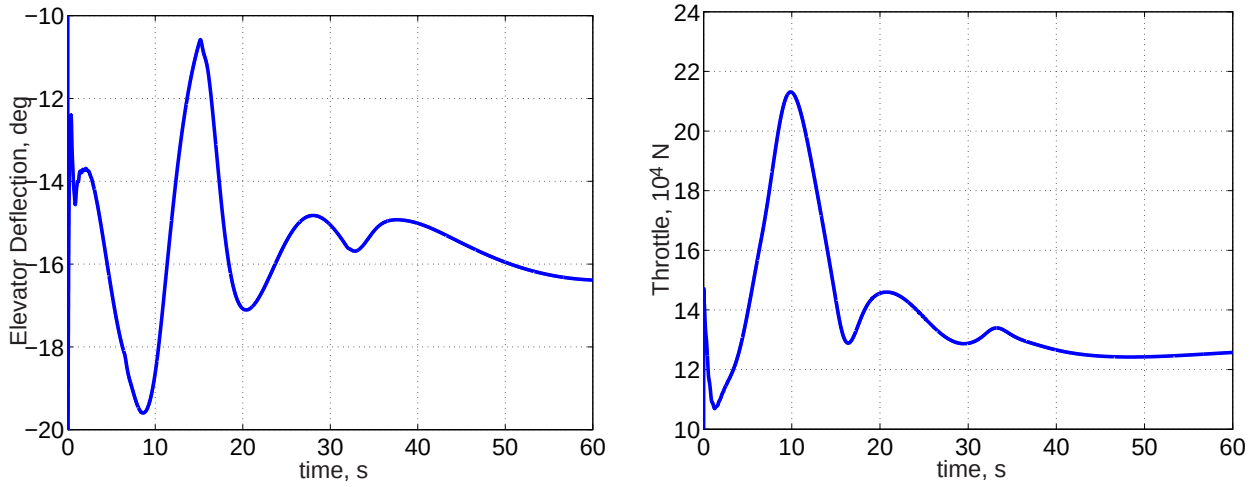

(a) Elevator (b) Throttle

Figure 17. Longitudinal flight controls, heavy weight condition, bank/climb command

angular velocities are shown in Figures 19, 20, and 21. Similar difficulties to the bank only command are seen in this simulation. However, due to the overall good control on total velocity, Eq. 27, Figure 19 (between 64.8 to 65.2$\frac{m}{s}$), and acceptable control on the flight path angle, Figure 16, there is less than a 5 m steady state error in altitude. Additionally, the desired Euler bank angle is achieved at steady state.

5. Bank and Climb at Empty Fuel State

To investigate the robustness of the proposed controller architecture, the same bank and climb trajectory of the previous section is repeated here, but at an empty fuel condition. Figure 22 shows the desired and actual response in flight path angle, altitude, and bank angle. While the bank angle response is similar to heavy fuel condition, Figure 16c, there are greater excursions in the flight path angle and altitude. These excursions are attributed to the outer-loop controller. The longitudinal and lateral control inputs are shown in Figures 23 and 24. The B reference frame linear and angular velocity trajectories (actual, commanded, desired) are shown in Figures 25, 26, and 27. An examination of the vertical velocity, Figure 25b, highlights a problem with applying the controller designed for the heavy weight to the light weight condition. In the

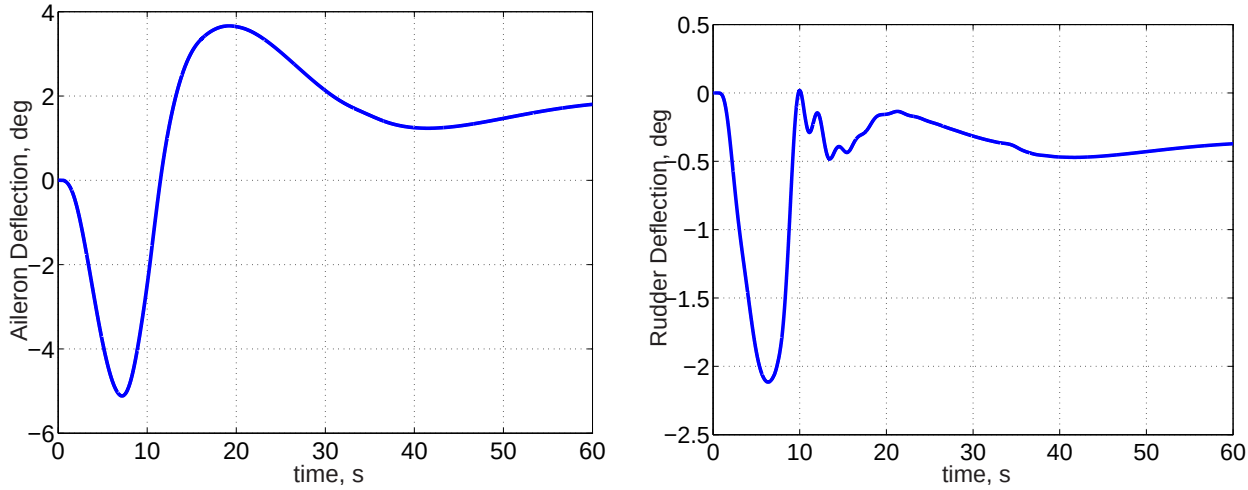

(a) Aileron (b) Rudder

Figure 18. Lateral flight controls, heavy weight condition, bank/climb command

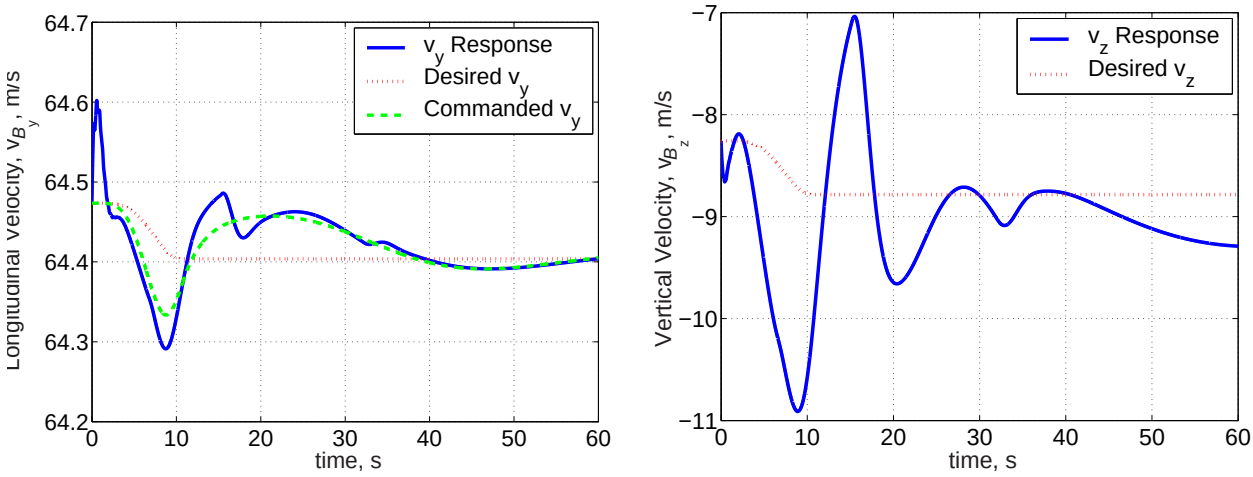

(a) Longitudinal velocity (b) Vertical velocity

Figure 19. B reference frame velocities, heavy weight condition, bank/climb command

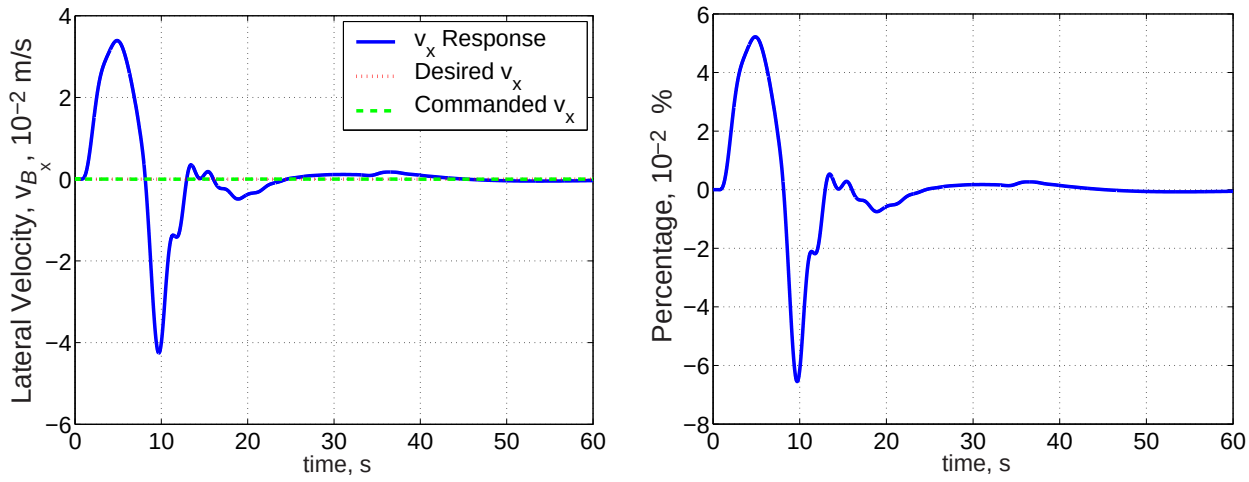

(a) Lateral velocity (b) Lateral velocity as a percentage of total velocity

Figure 20. *B* **reference frame lateral velocity, heavy weight condition, bank/climb command**

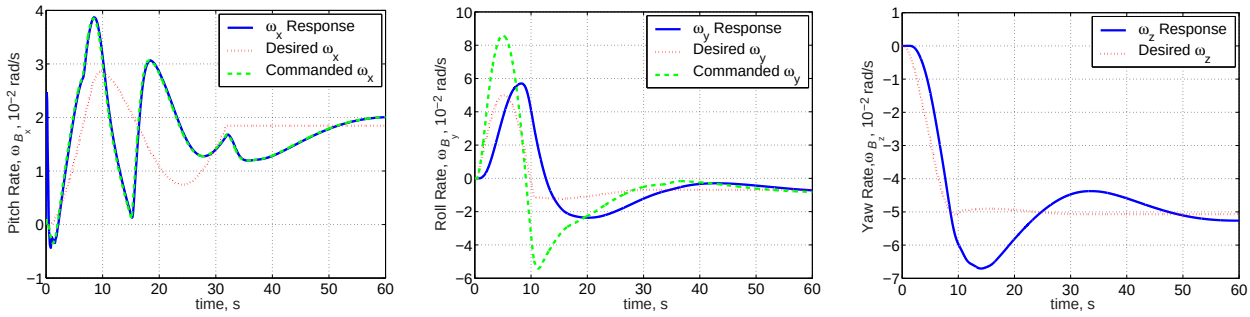

(a) Pitch Rate (b) Roll Rate (c) Yaw Rate

Figure 21. *B* **reference frame angular velocities, heavy weight condition, bank/climb command**

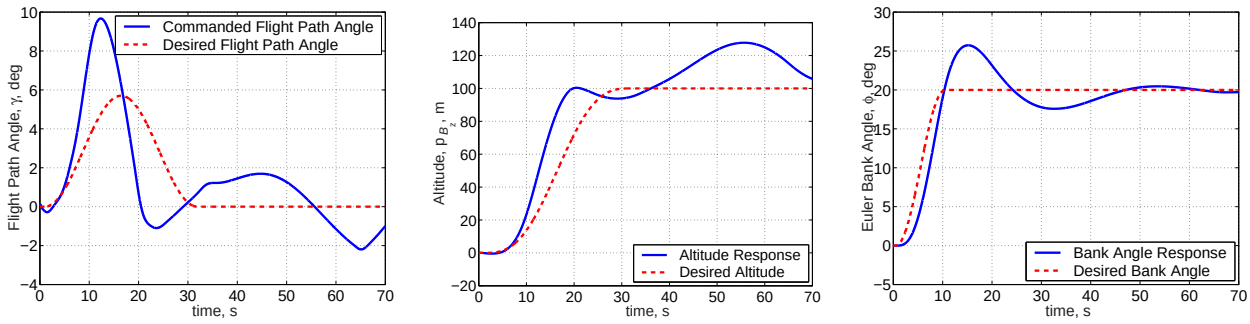

(a) Flight Path Angle (b) Altitude (c) Euler Bank Angle

Figure 22. Commanded flight path angle, altitude, and Euler angle for light weight condition, bank/climb command

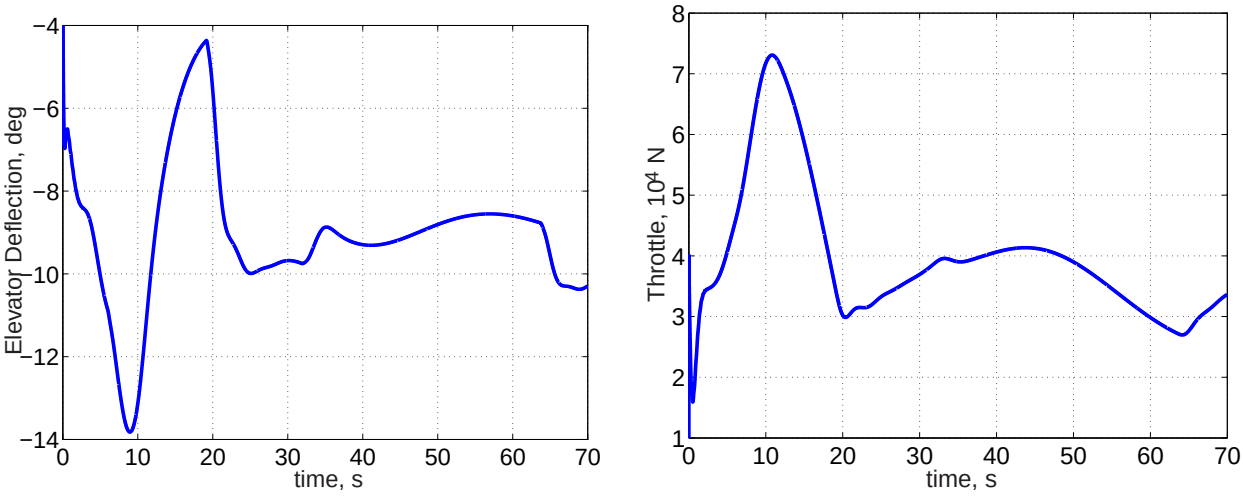

(a) Elevator (b) Throttle

Figure 23. Longitudinal flight controls, light weight condition, bank/climb command

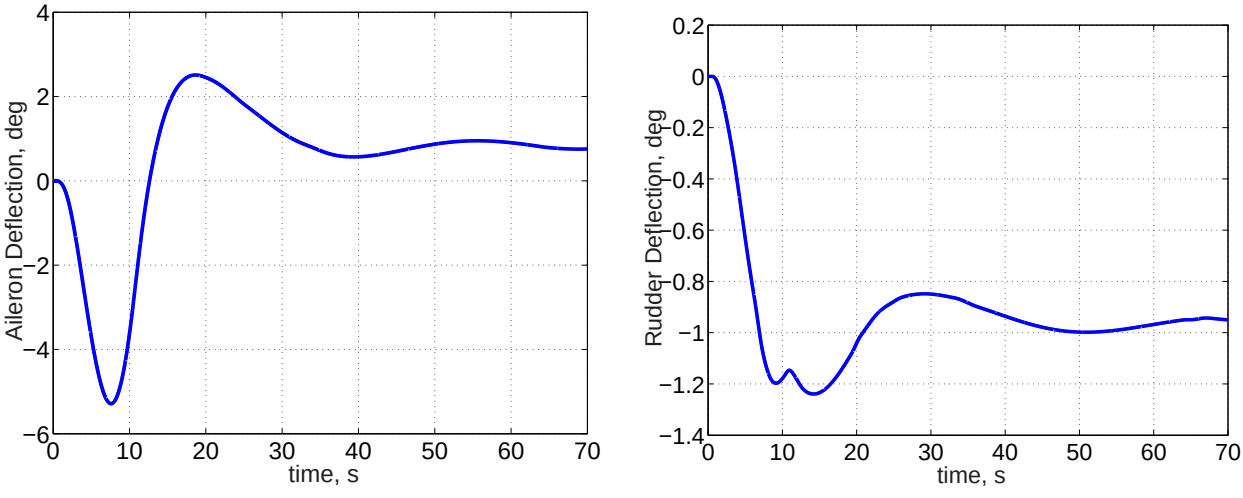

(a) Aileron (b) Rudder

Figure 24. Lateral flight controls, light weight condition, bank/climb command

outer-loop nonlinear transformation, Section III.D.3, the body angle-of-attack, α, is a derived and required parameter, based upon a steady state wings-level zero angle-of-attack, α_0, given in Eq. 48. The heavy weight controller was designed using a trim body body angle of attack, α_0 of 7.30° and presented in Table 10, and applied to the light weight condition here. Note, for a light weight condition, the trim body angle of attack, α_0, is 1.93°. Despite the resulting large discrepancy in α_0 and vertical velocities between the light and heavy weight conditions, the controller performs adequately for the significant change in mass, Table 10. This is because vertical velocity is not actively controlled and the other B reference frame velocities are not as significantly affected by α_0.

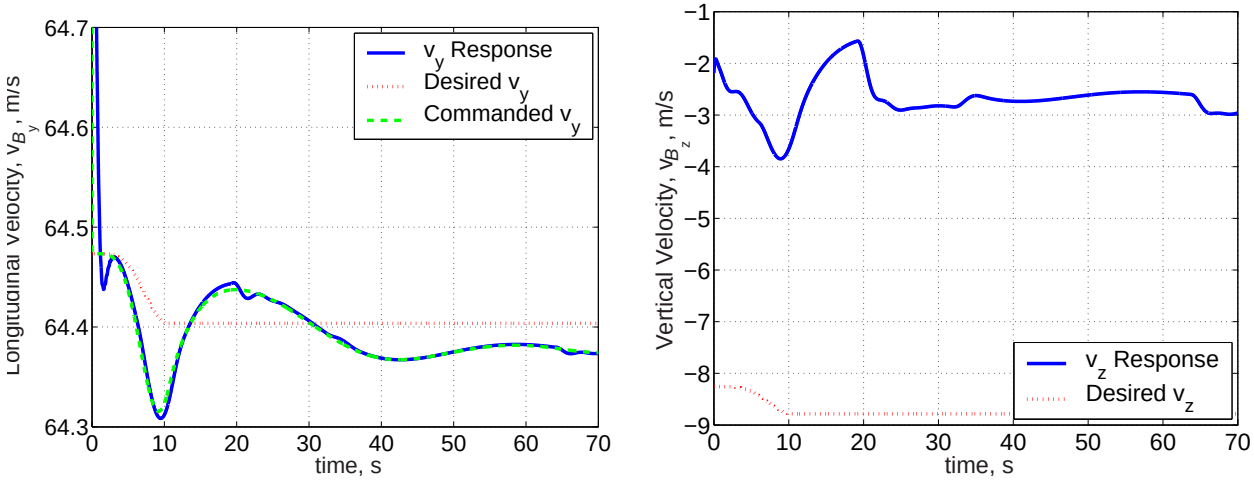

(a) Longitudinal velocity

(b) Vertical velocity

Figure 25. *B* **reference frame velocities, light weight condition, bank/climb command**

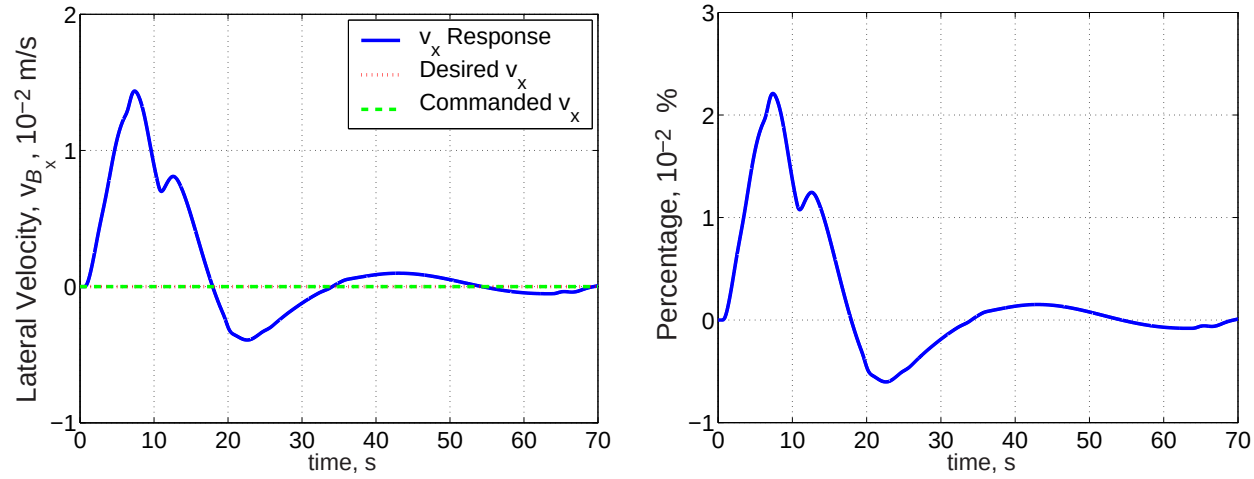

(a) Lateral velocity

(b) Lateral velocity as a percentage of total velocity

Figure 26. *B* **reference frame lateral velocity, heavy weight condition, bank/climb command**

6. Mission Profile Segment Case

A final representative mission profile segment simulation is presented here. The aircraft is commanded to perform the following sequence of maneuvers: climb and turn, roll out of turn and continue climbing, level off, level turn, descent and turn, roll out of turn and continue descending, and level off as seen in Figure 28. The altitude and associated flight path angle along with the Euler bank angle desired and actual trajectories are seen in Figures 29 and 30. Altitude tracking presents a maximum overshoot of 46 meters

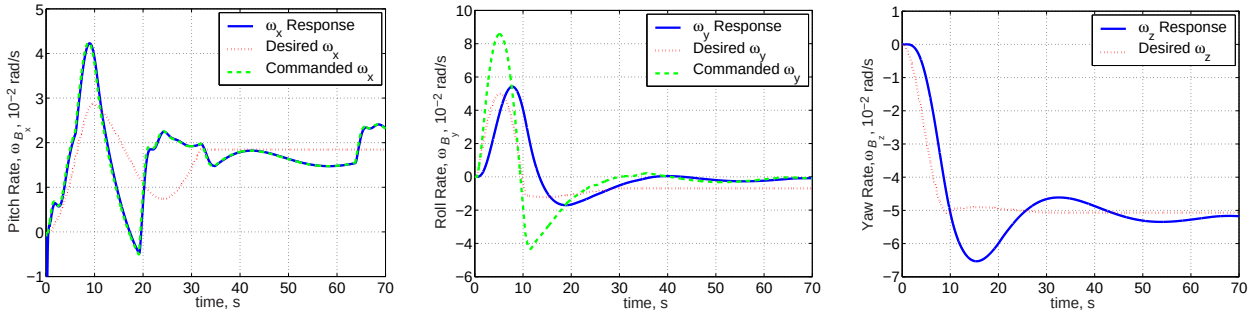

(a) Pitch Rate (b) Roll Rate (c) Yaw Rate

Figure 27. *B* **reference frame angular velocities, light weight condition, bank/climb command**

following the commanded climb. This overshoot occurs while the bank angle is settling to its commanded zero degree angle. The overshoot in altitude is acceptable given that this class of aircraft is expected to fly in the National Airspace System. Typical piloted aircraft flying under instrument flight rules (IFR) are required to maintain less than about 30 meter steady state altitude deviations and are allowed up to 60 meter temporary deviations. The corresponding longitudinal and lateral control inputs are seen in Figures 31 and 32. During the second portion of the commanded climb, an increase in throttle and decrease in elevator are seen (between 50 and 75 seconds) corresponding to the greater commanded climb rate ($6.67m/s$ at 25 seconds and $13.33m/s$ at 65 seconds). There is a steady state altitude error of less than 2 meters at 250 seconds and 4 meters at 400 seconds. Bank angle overshoots are less than 7.2° with excellent steady state tracking. The *B* reference frame desired, commanded, and actual velocities are seen in Figures 33, 34,

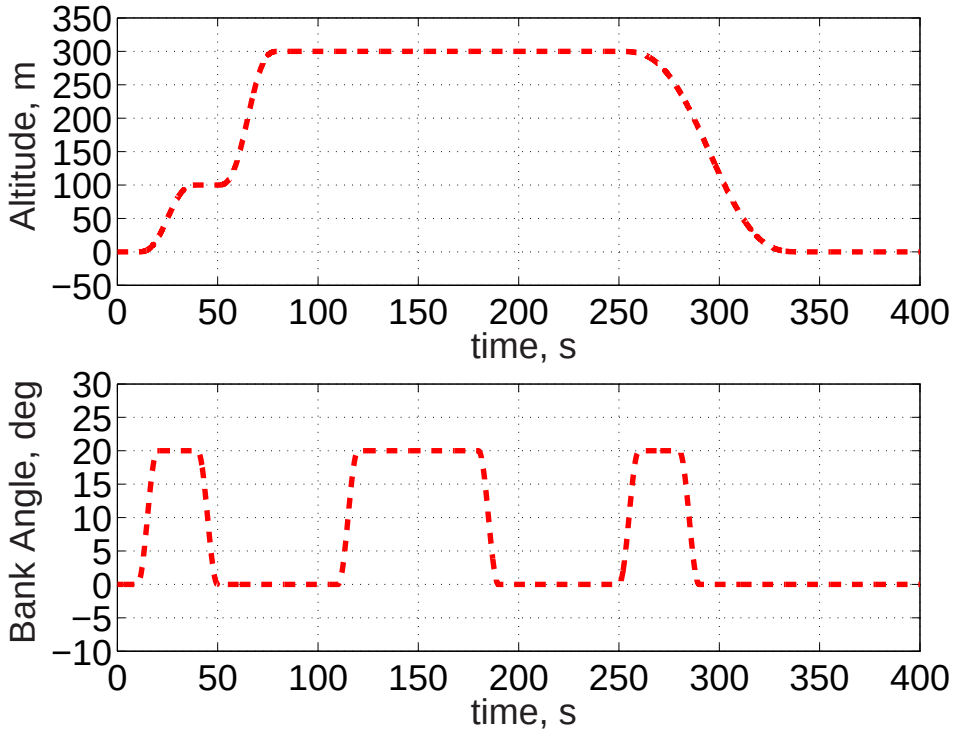

Figure 28. Representative mission profile segment

35, and 36. As with previous results there is excellent tracking of the commanded longitudinal velocity, Figure 33b, and pitch rate, Figure 35a. Again tracking error between the desired and commanded values in the longitudinal motion are attributed to outer-loop controller architecture. For the lateral motion the

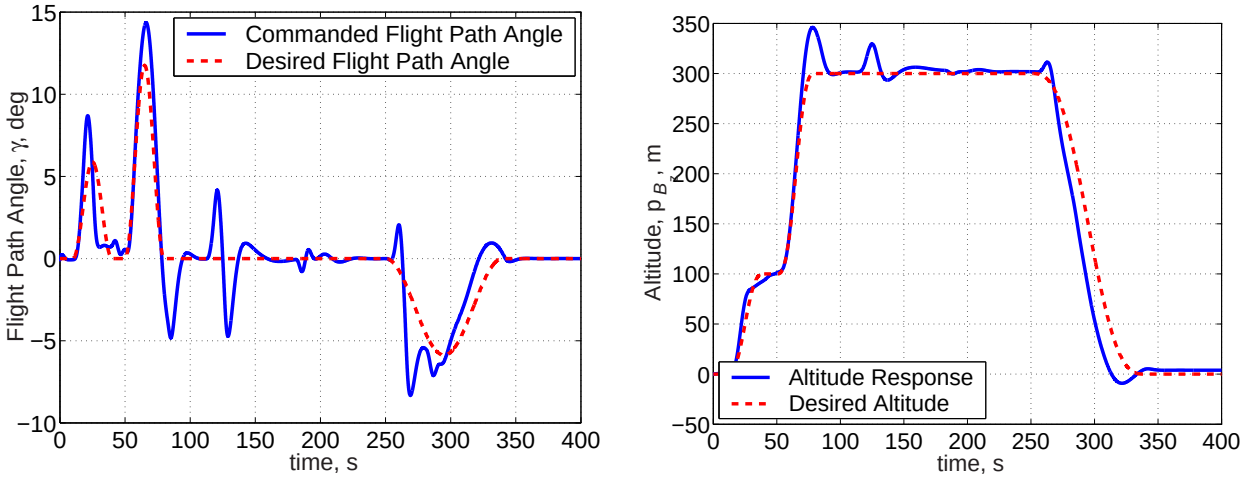

(a) Flight path angle

(b) Altitude

Figure 29. Commanded flight path angle and altitude for heavy weight condition

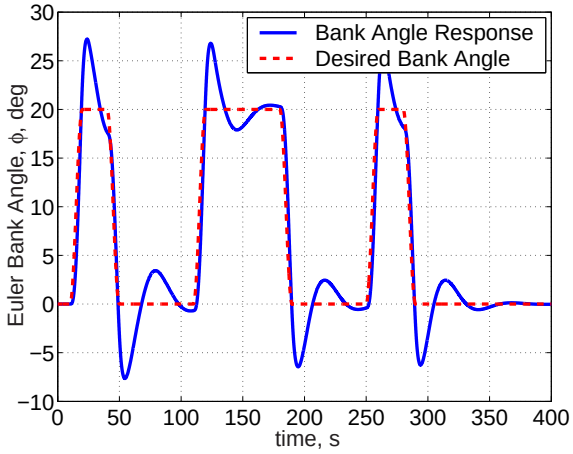

Figure 30. Commanded Euler bank angle for heavy weight condition

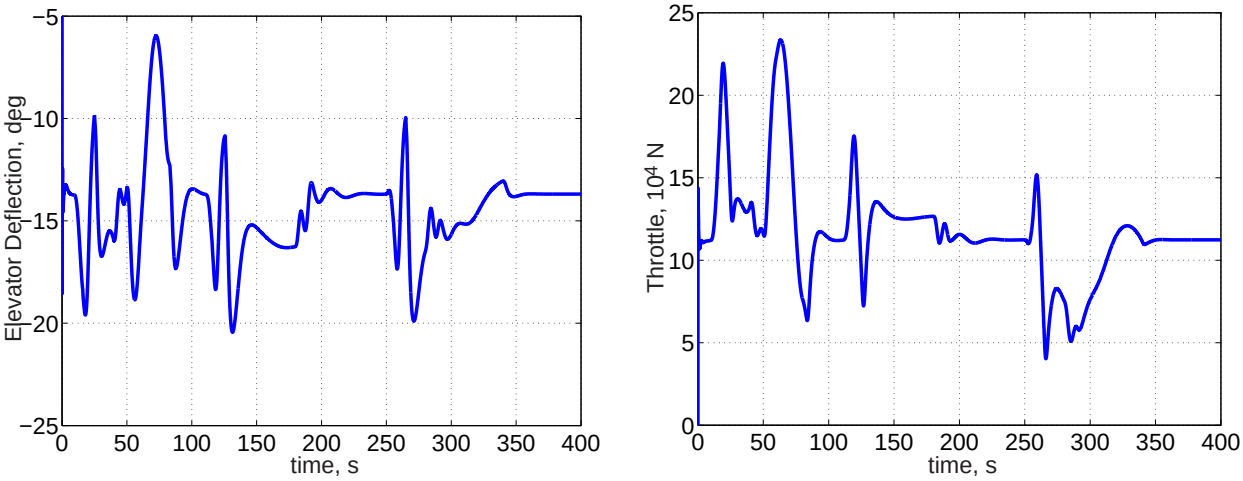

(a) Elevator

(b) Throttle

Figure 31. Longitudinal flight controls, heavy weight condition

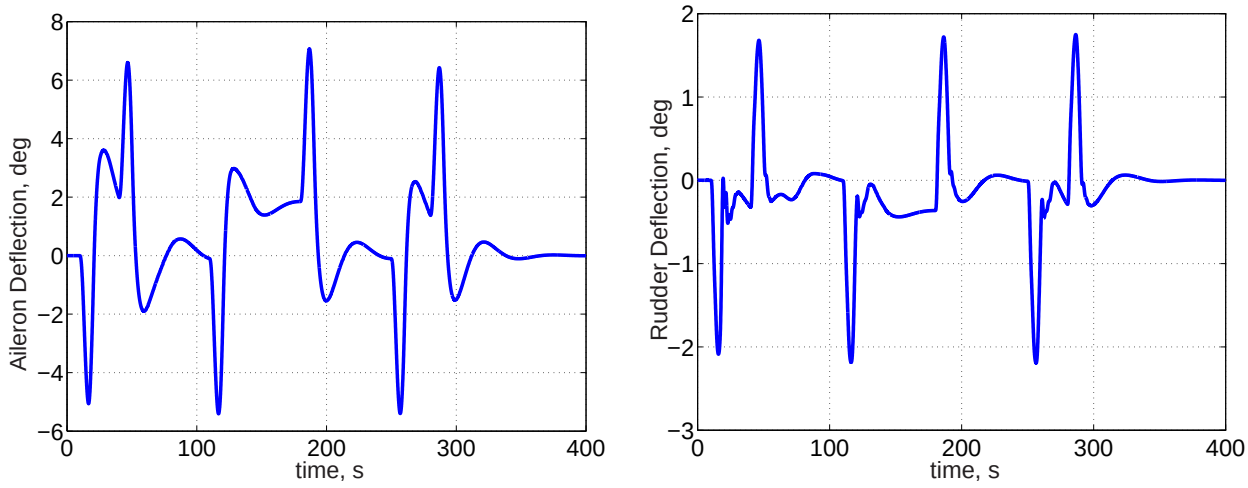

(a) Aileron (b) Rudder

Figure 32. Lateral flight controls, heavy weight condition

sideslip velocity, Figure 33a, is seen to be below $0.04m/s$ or 0.05% of the total velocity, V. Additionally the roll rate (Figure 35b) has acceptable tracking and the yaw rate (Figure 35c), while not directly controlled, has relatively good and stable tracking of the desired trajectory.

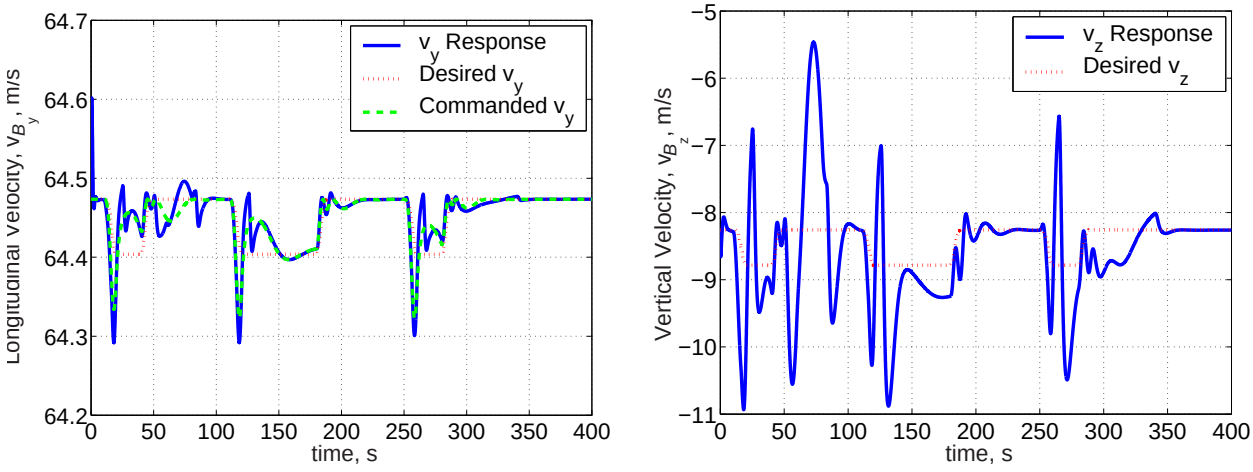

(a) Longitudinal velocity (b) Vertical velocity

Figure 33. B reference frame velocities, heavy weight condition

V. Concluding Remarks

The control architecture was shown numerically to track altitude and bank angle changes in the presence of smooth air, full elastic state feedback, and perfect sensors. The purpose of these studies was not to design a perfect controller, but rather demonstrate the viability of the proposed method. In such, there is more tuning which could be accomplished for tighter trajectory control. The inner- and outer-loop architecture demonstrated an effective means for accomplishing trajectory control of very flexible aircraft. While more complex, the proposed architecture shows to be much easier to achieve stable tracking as compared to more traditional methods. Furthermore, the separation of longitudinal and lateral motion control handled by separate controllers proved to be very effective. Finally, while not presented here, the general trends of increased integral gain destabilizing system response and increased derivative gain stabilizing and slowing

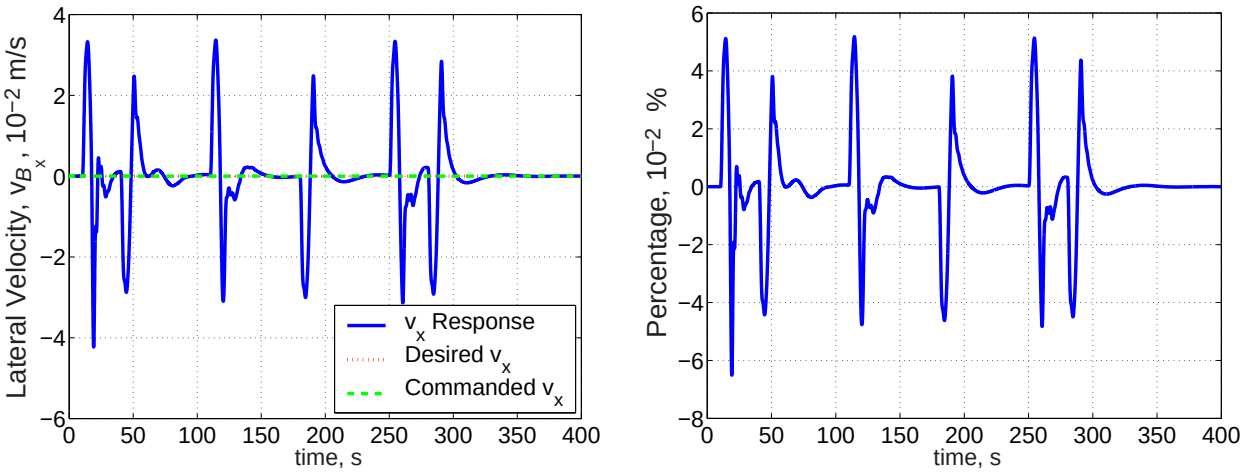

(a) Lateral velocity

(b) Lateral velocity as a percentage of total velocity

Figure 34. *B* **reference frame lateral velocity, heavy weight condition**

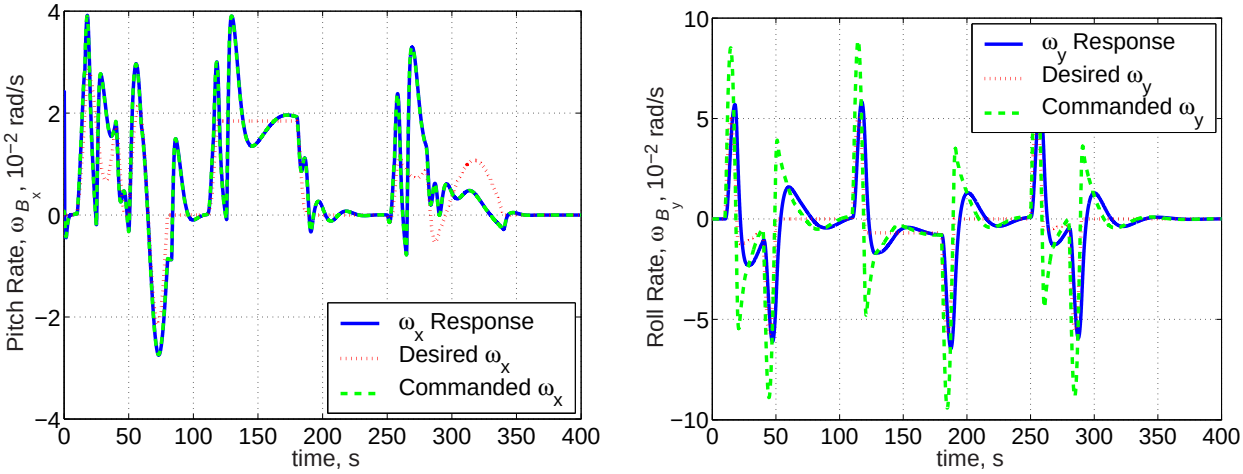

(a) Pitch rate

(b) Roll rate

Figure 35. *B* **reference frame angular velocities, heavy weight condition**

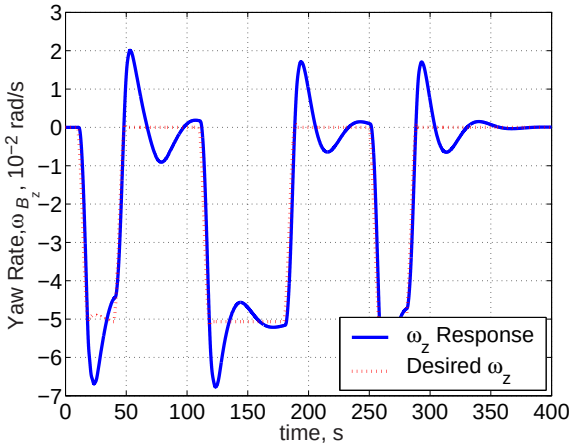

Figure 36. Yaw rate, *B* **reference frame angular velocity, heavy weight condition**

system response were seen in the development of the outer-loop nonlinear gains.

Acknowledgments

The views expressed in this article are those of the authors and do not reflect the official policy or position of the United States Air Force, Department of Defense, or the U.S. Government.

References

[1]Noll, T. E., Brown, J. M., Perez-Davis, M. E., Ishmael, S. D., Tiffany, G. C., and Gaier, M., "Investigation of the Helios Prototype Aircraft Mishap," Tech. rep., NASA, January 2004.

[2]Tilmann, C. P., Flick, P. M., Martin, C. A., and Love, M. H., "High-Altitude Long Endurance Technologies for SensorCraft," *RTO AVT Symposium on "Novel Vehicle Concepts and Emerging Vehicle Technologies"*, Brussels, Belgium, April 7–10 2003, MP-104-P-26-1.

[3]Whitson, S., "The Proteus, Giving Shape to Forms Unknown," *Private Pilot*, Vol. 33, No. 12, December 1998, pp. 44–50.

[4]annon., "Unmanned Aircraft Systems Roadmap 2005-2030," Tech. rep., Office of the Secretary of Defense, Department of Defense, 4 August 2005.

[5]Schroer, R., "Stability and Control [A Century of Powered Flight 1903-2003]," *IEEE Aerospace and Electronic Systems Magazine*, Vol. 18, No. 7, July 2003, pp. 37–42.

[6]Nelson, R. C., *Flight Stability and Automatic Control*, Princeton University Press, Boston, 2nd ed., 1998.

[7]Mukhopadhyay, V., "Historical Perspective on Analysis and Control of Aeroelastic Responses," *Journal of Guidance, Control, and Dynamics*, Vol. 26, No. 5, September-October 2003, pp. 673–684.

[8]Newman, B. and Buttrill, C., "Conventional Flight Control for an Aeroelastic Relaxed Static Stability High-Speed Transport," *AIAA Guidance, Navigation and Control Conference*, Baltimore, Maryland, August 7–10 1995, pp. 717–726, AIAA Paper No. 95-3250-CP.

[9]Tuzcu, I., *Dynamics and Control of Flexible Aircraft*, Ph.D. thesis, Virgina Polytechmic Institute and State University, Blacksburg, Virginia, December 2001, PhD Dissertation.

[10]Meirovitch, L. and Tuzcu, I., "Unified Theory for the Dynamics and Control of Maneuvering Flexible Aircraft," *AIAA Journal*, Vol. 42, No. 4, April 2004, pp. 714–727.

[11]Pedro, J. O. and Bigg, C. G., "Development of a Flexible Embedded Aircraft/Control System Simulation Facility," *AIAA Atmospheric Flight Mechanics Conference and Exhibit*, AIAA, San Francisco, CA, August 15-18 2005, AIAA Paper No. 2005-5889.

[12]Cesnik, C. E. S. and Ortega-Morales, M., "Active Aeroelastic Tailoring of Slender Flexible Wings," *International Forum on Aeroelasticity and Structural Dynamics*, Madrid, Spain, 5 June – 7 June 2001.

[13]Chavez, F. R. and Schimdt, D. K., "Systems Approach to Characterizing Aircraft Aeroelastic Model Variation for Robust Control Applications," *AIAA Guidance, Navigation, and Control Conference and Exhibit*, Montreal, Canada, August 6–9 2001, AIAA Paper No. 2001-4020.

[14]Kron, A., deLafontaine, J., and Alazard, D., "Robust 2-DOF H-infinity Controller for Highly Flexible Aircraft: Design Methodology and Numerical Results," *The Canadian Aeronautics and Space Journal*, Vol. 49, No. 1, March 2003, pp. 19–29.

[15]Li, X. and Agarwal, R. K., "Application of Reduced-Order-Models to Robust Control of the Dynamics of a Flexible Aircraft," *AIAA Guidance, Navigation, and Control Conference and Exhibit*, Austin, Texas, August 11–14 2003, AIAA Paper No. 2003-5504.

[16]Goman, M., Sidoryuky, M., and Ustinovz, A., "Control Law Design for Flexible Aircraft: Comparison of the H1-based and Classical Methods," *AIAA Atmospheric Flight Mechanics Conference and Exhibit*, AIAA, San Francisco, CA, August 15-18 2005, AIAA Paper No. 2005-6265.

[17]Dardenne, I. and Ferreres, G., "Design of a Flight Control System for a Highly Flexible Aircraft using Convex Synthesis," *ICAS 98 Proceedings; 21st Congress of the International Council of the Aeronautical Sciences*, Melbourne, Victoria, Australia, September 13–18 1998, ICAS-98-1,5,1.

[18]Patil, M., *Nonlinear Aeroelastic Analysis. Flight Dynamics, and Control of a Complete Aircraft*, Ph.D. thesis, Georgia Institute of Technology, Atlanta, Georgia, May 1999, PhD Dissertation.

[19]Patil, M. J. and Hodges, D. H., "Output Feedback Control of the Nonlinear Aeroelastic Response of a Slender Wing," *Journal of Guidance, Control and Dynamics*, Vol. 25, No. 2, March-April 2002, pp. 302–308.

[20]Calise, A. J., Kim, N., and Buffington, J. M., "Adaptive Compensation for Flexible Dynamics," *AIAA Guidance, Navigation, and Control Conference and Exhibit*, AIAA, Monterey, CA, August 5-8 2002, AIAA Paper No. 2002-4917.

[21]Krishnaswamy, K. and Bugajski, D., "Inversion Based Multibody Control - Launch Vehicle with Fuel Slosh," *AIAA Atmospheric Flight Mechanics Conference and Exhibit*, AIAA, San Francisco, CA, August 15-18 2005, AIAA Paper No. 2005-6149.

[22]Gregory, I. M., "Dynamic Inversion to Control Large Flexible Transport Aircraft," *AIAA Guidance, Navigation, and Control Conference and Exhibit*, Boston, Massachusetts, August 10–12 1998, pp. 1224–1232, AIAA Paper No. 98-4323.

[23]Gregory, I. M., "Stability Result for Dynamic Inversion Devised to Control Large Flexible Aircraft," *AIAA Guidance, Navigation, and Control Conference and Exhibit*, Montreal, Quebec, August 6–9 2001, AIAA Paper No. 2001-4284.

[24]Gregory, I. M., "Modified Dynamic Inversion to Control Large Flexible Transport Aircraft - What's Going On?" *AIAA Guidance, Navigation, and Control Conference and Exhibit*, Portland, Oregon, August 9–11 1999, pp. 392–402, AIAA Paper No. 99-3998.

[25]Gregory, I. M., *Design and Stability Analysis of an Integrated Controller for Highly Flexible Advanced Aircraft Utilizing the Novel Nonlinear Dynamic Inversion*, Ph.D. thesis, California Institute of Technology, Pasadena, California, 2005, PhD Dissertation.

[26]Cesnik, C. E. S. and Brown, E. L., "Active Wing Warping Control of a Joined-Wing Airplane Configuration," *Proceedings of the 44th AIAA/ASME/ASCE/AHS Structures, Structural Dynamics, and Materials Conferences*, Norfolk, Virgina, April 7–10 2003, AIAA Paper No. 2003-1715.

[27]Stevens, B. L. and Lewis, F. L., *Aircraft Control and Simulation*, John Wiley & Sons, Inc., New York, 1992.

[28]Phillips, W. F., Hailey, C. E., and Gebert, G. A., "A Review of Attitude Kinematics for Aircraft Flight Simulation," *AIAA Modeling and Simulation Technologies Conference and Exhibit*, AIAA, Denver, CO, August 14 - 17 2000, AIAA Paper No. 2000-4302.

[29]Peters, D. and Johnson, M. J., "Finite-State Airloads for Deformable Airfoils on Fixed and Rotating Wings," *Aeroelasticity and Fluid/Structure Interation, Proceedings of the Winter Annual Meeting*, ASME, November 6–11 1994.

[30]Peters, D. A. and Cao, W., "Finite State Induced Flow Models Part I: Two-Dimensional Thin Airfoil," *Journal of Aircraft*, Vol. 32, No. 2, March-April 1995, pp. 313–322.

[31]Brown, E. L., *Integrated Strain Actuation in Aircraft with Highly Flexible Composite Wings*, Ph.D. thesis, Massachusetts Institute of Technology, Boston, Massachusetts, June 2003, PhD Dissertation.

[32]Shearer, C. M. and Cesnik, C. E. S., "Nonlinear Flight Dynamics of Very Flexible Aircraft," *AIAA Atmospheric Flight Mechanics Conference and Exhibit*, AIAA, San Fransisco, CA, August 15 - 18 2005, AIAA Paper No. 2005-5805.

[33]Shearer, C. M., *Coupled Nonlinear Flight Dynamics, Aeroelasticity, and Control of Very Flexible Aircraft*, Ph.D. thesis, The University of Michigan, Ann Arbor, MI, 2006, PhD Dissertation.

[34]Arora, J. S., *Introduction to Optimum Design*, McGraw-Hill, Inc., 1989.

[35]Shearer, C. M. and Cesnik, C. E. S., "Modified Generalized-α Method for Integrating Governing Equations of Very Flexible Aircraft," *AIAA 47th AIAA/ASME/ASCE/AHS/ASC Structures, Structural Dynamics, and Materials Conference*, AIAA, May 1 - 4 2006, AIAA Paper No. 2006-1747.

[36]Jansen, K. E., Whiting, C. H., and Hulbert, G. M., "A Generalized-α Method for Integrating the Filtered Navier-Stokes Equations with a Stabilized Finite Element Method," *Computer Methods in Applied Mechanics and Engineering*, Vol. 190, No. 3-4, 27 October 2000, pp. 305–319.

[37]Chung, J. and Hulbert, G. M., "A Time Integration Algorithm for Structural Dynamics With Improved Numerical Dissipation: The Generalized-α Method," *Journal of Applied Mechanics*, Vol. 60, June 1993, pp. 371–375.

[38]annon., "Flying Qualities of Piloted Vehicles," Military standard, United States Department of Defense, 1987.

[39]Stengel, R. F., *Flight Dynamics*, Princeton University Press, Princeton, New Jersey, 2004.

[40]Heffley, R. K., Hanson, G. D., Jewell, W. F., and Clement, W. F., "Analysis of Pilot Control Strategy," Contractor Report NASA CR-170399, NASA, April 1983.

[41]Heffley, R. K. and Schulman, T. M., "Derivation of Human Pilot Control Laws Based on Literal Interpretation of Pilot Training Literature," *AIAA Guidance and Control Conference*, AIAA, Albuquerque, NM, August 19-21 1981, AIAA Paper No. 1981-1822.

[42]Franklin, G. F., Powell, J. D., and Emami-Naeini, A., *Feedback Control of Dynamic Systems*, Addison-Wesley Publishing Company, 3rd ed., 1994.

[43]J. D. Anderson, J., *Introduction to Flight*, McGraw-Hill Book Company, 2nd ed., 1985.

[44]Ziegler, J. G. and Nichols, N. B., "Optimum Settings for Automatic Controllers," *Transactions of the ASME*, Vol. 64, November 1942, pp. 759–768.

[45]Ziegler, J. G. and Nichols, N. B., "Process Lags in Automatic-Control Circuits," *Transactions of the ASME*, Vol. 65, No. 5, July 1943, pp. 433–444.

[46]Bugajski, D. J. and Enns, D. F., "Nonlinear Control Law with Application to High Angle-of-Attack Flight," *Journal of Guidance, Control and Dynamics*, Vol. 15, No. 3, May-June 1992, pp. 761–767.

[47]Adams, R. J., Buffington, J. M., and Banda, S. S., "Design of Nonlinear Control Laws for High Angle-of-Attack Flight," *Journal of Guidance, Control and Dynamics*, Vol. 17, No. 4, July-August 1994, pp. 737–746.

[48]Snell, S. A., Enns, D. F., and Jr., W. L. G., "Nonlinear Inversion Flight Control for a Supermaneuverable Aircraft," *Journal of Guidance, Control and Dynamics*, Vol. 15, No. 4, July-August 1992, pp. 976–984.

[49]Al-Hiddabi, S. A., *Position Tracking and Path Following for Flight Vehicles using Nonlinear Control*, Ph.D. thesis, The University of Michigan, Ann Arbor, MI, 2000, PhD Dissertation.

[50]Al-Hiddabi, S. A. and McClamroch, N. H., "Tracking and Maneuver Regulation Control for Nonlinear Nonminimum Phase Systems: Application to Flight Control," *IEEE Transactions on Control Systems Technology*, Vol. 10, No. 6, November 2002, pp. 780–792.

[51]Slotine, J. E. and Li, W., *Applied Nonlinear Control*, Prentice-Hall, Inc., Englewood Cliffs, NJ 07632, 1991.

[52]Khalil, H. K., *Nonlinear Systems*, Prentice-Hall Inc., Upper Saddle River, NJ 07458, 3rd ed., 2002.

[53]Bernstein, D. S., *Matrix Mathematics: Theory, Facts, and Formulas with Application to Linear Systems Theory*, Princeton University Press, 1st ed., 2005.

[54]Barrett, M., Blue, P., Bugajski, D., Enns, D., Hendrick, R., Jackson, M., Morton, B., Stein, G., Bessollo, J., Virnig, J., Walker, G., Colgren, R., Tait, P., and Smith, R., "Application of Multivariable Control Theory to Aircraft Control Laws," Final Report WL-TR-96-3099, Flight Dynamics Directory Wright Laboratory U.S. Air Force, Air Force Material Command, Wright Patterson AFB, OH 45433-7562, May 1996.

[55]Ito, D., Georgie, J., Valasek, J., and Ward, D. T., "Re-Entry Vehicle Flight Controls Design Guidelines: Dynamic Inversion," Final Technical Report NAG9-1085, Flight Simulation Laboratory Texas Engineering Experiment Station, Texas A&M University, College Station, TX, May 2001.

[56]Freudenberg, J., "AERO 580 Linear Feedback Notes," The University of Michigan, Ann Arbor, Michigan, 2004, Class Notes.

[57]Kreyszig, E., *Advanced Engineering Mathematics*, John Wiley & Sons, Inc., New York, 7th ed., 1993.
[58]Reid, J. G., *Linear System Fundamentals Continuous and Discrete, Classic and Modern*, McGraw-Hill, Inc., New York, 1983.